SEMI-AUTOMATIC IMAGE SEGMENTATION AND 3D VISUALIZATION OF NASOPHARYNGEAL CARCINOMA

WEERAYUTH CHANAPAI

A THESIS SUBMITTED IN PARTIAL FULFILLMENT
OF THE REQUIREMENTS FOR
THE DEGREE OF MASTER OF ENGINEERING
(BIOMEDICAL ENGINEERING)
FACULTY OF GRADUATE STUDIES
MAHIDOL UNIVERSITY
2010

Thesis
entitled

SEMI-AUTOMATIC IMAGE SEGMENTATION AND 3D VISUALIZATION OF NASOPHARYNGEAL CARCINOMA

……
Mr. Weerayuth Chanapai
Candidate

……
Lect. Panrasee Ritthiphavat,
D.Eng. (Mechanical Engineering)
Major advisor

……
Asst.Prof. Thongchai Bhongmakapat,
M.D. (Otolaryngology)
Co-advisor

……
Asst.Prof. Lojana Tuntiyatorn,
M.D. (Radiology)
Co-advisor

……
Prof. Banchong Mahaisavariya,
M.D., Dip Thai Board of Orthopedics
Dean
Faculty of Graduate Studies

……
Asst.Prof. Jackrit Suthakorn,
Ph.D. (Robotics)
Chair
Master of Engineering Program in
Biomedical Engineering
Faculty of Engineering
Mahidol University

Thesis
entitled

SEMI-AUTOMATIC IMAGE SEGMENTATION AND 3D VISUALIZATION OF NASOPHARYNGEAL CARCINOMA

was submitted to the Faculty of Graduate Studies, Mahidol University
for the degree of Master of Engineering (Biomedical Engineering)
on
June 11, 2010

……
Mr. Weerayuth Chanapai
Candidate

……
Lect. Songpol Ongwattanakul,
Ph.D. (Computer Enginnering)
Chair

……
Asst.Prof. Lojana Tuntiyatorn,
M.D. (Radiology)
Member

……
Lect. Panrasee Ritthiphavat,
D.Eng. (Mechanical Engineering)
Member

……
Lect. Danai Laksameethanasan,
D.Sc. (Technology)
Member

……
Asst.Prof. Thongchai Bhongmakapat,
M.D. (Otolaryngology)
Member

……
Prof. Banchong Mahaisavariya,
M.D. Dip Thai Board of Orthopedics
Dean
Faculty of Graduate Studies
Mahidol University

……
Asst.Prof. Rawin Raviwongse,
Ph.D. (Engineering Management)
Dean
Faculty of Engineering
Mahidol University

ACKNOWLEDGEMENTS

The success of this thesis can be achieved by the attentive support from my thesis advisor, Dr. Panrasee Ritthipavat who gave me invaluable suggestions, continuous support and encouragement during the period of my study. Associate Professor Thongchai Bhongmakapat and Associate Professor Lojana Tuntiyatorn who was my co-adviser for their time and effort in providing the author with their continual guidance and valuable recommendation which make me achieving this success.

I would like to express my sincere gratitude to the committee members: Dr. Songpol Ongwattanakul and Dr. Danai Laksameethanasan for their comments and kind suggestions.

I am particularly indebted to Ramathibodi Hospital for their co-operation and generous assistance.

I am grateful and deeply appreciate to my family for all kinds of their supports and entirely care which made this thesis possible and enabled me to undertake this thesis successfully.

I would like to thanks Graduate Studies Mahidol University Alumni Association who gave the partial support. Finally, thanks also be given to the Faculty of Engineering, Mahidol University in enabling me to undertake this research.

Weerayuth Chanapai

SEMI-AUTOMATIC IMAGE SEGMENTATION AND 3D VISUALIZATION OF NASOPHARYNGEAL CARCINOMA

WEERAYUTH CHANAPAI 4936234 EGBE/M

M.Eng. (BIOMEDICAL ENGINEERING)

THESIS ADVISORY COMMITTEE: PANRASEE RITTHIPRAVAT, D.Eng., THONGCHAI BHONGMAKAPAT, M.D., LOJANA TUNTIYATORN, M.D.

ABSTRACT

This research aimed at developing software for semi-automatic image segmentation and 3D visualization of nasopharyngeal carcinoma (NPC) from CT images. A segmentation technique based on a self-organizing map (SOM) was proposed in order to extract the tumor region from the images. Initial tumor pixels, called seed points, were specified. Information from the seed points was used to determine the extent of the tumor in a CT image. The proposed segmentation algorithm was then compared with the traditional seeded region growing approach and standard ground truth images specified by radiologists. The results from the segmentation showed that the proposed technique was superior to the traditional approach in that it provided the highest segmentation performance.

After the tumor regions were selected from the images, a 3D model of the tumor was constructed and presented in the virtual skull which was created from surface and volume rendering techniques. Precision of 3D reconstruction was investigated by comparing 3 geometrical models with their 3D reconstructed models. The results from the 3D model showed that the volume of each 3D reconstructed model was slightly larger than the actual model. This is because the quantization effect.

The developed software from this study can help physicians in diagnosis and treatment planning. Useful information such as common site, cell growth and invasion patterns can be easily observed. In addition, physicians can compare the 3D models of pre and post-treatments in order to evaluate treatment efficiency.

KEY WORDS: NASOPHARYNGEAL CARCINOMA/ SELF-ORGANIZING MAP/ SURFACE RENDERING/ VOLUME RENDERING

76 pages

การจำแนกภาพแบบกึ่งอัตโนมัติและสร้างภาพจำลองสามมิติของเนื้อเยื่อมะเร็งช่องคอหลังโพรงจมูก

SEMI-AUTOMATIC IMAGE SEGMENTATION AND 3D VISUALIZATION OF NASOPHARYNGEAL CARCINOMA

วีระยุทธ ชนะภัย 4936234 EGBE/M

วศ.ม. (วิศวกรรมชีวการแพทย์)

คณะกรรมการที่ปรึกษาวิทยานิพนธ์ : ปัณรสี ฤทธิประวัติ, D.Eng., ธงชัย พงศ์มฆพัฒน์, M.D., โลจนา ตันติยาทร, M.D.

บทคัดย่อ

งานวิจัยนี้มีวัตถุประสงค์เพื่อพัฒนาซอฟต์แวร์สำหรับการจำแนกภาพแบบกึ่งอัตโนมัติและสร้างภาพจำลองสามมิติของเนื้อเยื่อมะเร็งช่องคอหลังโพรงจมูกจากภาพซีที เทคนิคการจำแนกภาพโดยใช้แผนผังเรียนรู้แบบจัดตัวเองหรือ Self-Organizing Map (SOM) ได้ถูกนำเสนอเพื่อจำแนกพื้นที่เนื้อเยื่อมะเร็งในภาพ โดยจุดเริ่มต้นของการจำแนกจะถูกกำหนดโดยผู้ใช้ ซึ่งข้อมูลที่ได้จากจุดเริ่มต้นดังกล่าวถูกนำมาใช้ในการกำหนดขอบเขตเนื้อเยื่อมะเร็งในภาพซีที ผลการจำแนกภาพของ อัลกอริธึมที่นำเสนอจะถูกนำไปเปรียบเทียบกับผลการจำแนกภาพโดยเทคนิคการขยายพื้นที่หรือ Seeded region growing แบบดั้งเดิมและขอบเขตเนื้อเยื่อมะเร็งที่ถูกกำหนดโดยรังสีแพทย์ผู้มีประสบการณ์ ผลการเปรียบเทียบแสดงให้เห็นว่าอัลกอริธึมที่นำเสนอให้ผลการจำแนกภาพเนื้อเยื่อมะเร็งช่องคอหลังโพรงจมูกได้อย่างถูกต้องมากกว่าเทคนิคเดิม หลังจากเนื้อเยื่อมะเร็งถูกจำแนก รูปจำลอง 3 มิติของเนื้อเยื่อมะเร็งจะถูกสร้างขึ้นและถูกแสดงในกะโหลกศีรษะเสมือนที่สร้างขึ้นจากการเรนเดอร์พื้นผิวจำลองและการเรนเดอร์ปริมาตรจำลอง ความถูกต้องของแบบจำลอง 3 มิติถูกทำการศึกษาโดยการเปรียบเทียบระหว่างแบบจำลองทางเรขาคณิตจำนวน 3 แบบ และภาพจำลองสามมิติของแต่ละแบบจำลอง ผลการศึกษาพบว่าแบบจำลอง 3 มิติที่สร้างขึ้นให้ปริมาตรที่ใหญ่กว่าวัตถุจริง เนื่องจากผลของควอนไตเซชัน (quantization effect) ซอฟท์แวร์ที่พัฒนาขึ้นนี้ช่วยให้แพทย์สามารถวินิจฉัยและวางแผนการรักษา รวมถึงสามารถสังเกตข้อมูลเนื้อเยื่อมะเร็งที่เป็นประโยชน์ เช่น บริเวณที่พบมะเร็งบ่อย, การเติบโตของเซลล์ รูปแบบการแพร่กระจาย นอกจากนี้แพทย์สามารถใช้แบบจำลอง 3 มิติ ในการเปรียบเทียบผลก่อนและหลังการรักษาเพื่อประเมินประสิทธิภาพการรักษาได้อีกด้วย

76 หน้า

CONTENTS

CONTENTS (cont.)

LIST OF TABLES

LIST OF FIGURES

LIST OF FIGURES (cont.)

LIST OF FIGURES (cont.)

LIST OF FIGURES (cont.)

LIST OF FIGURES (cont.)

LIST OF ABBREVIATION

a	Minimum intensity
b	Maximum Intensity
BMU	Best matching unit
C	Constant
CR	Corresponding Ratio
D(i,j,k)	derivative of density function of pixel *(i,j,k)*
D	Original diameter of real object
D	Diameter of object image
d_k	Euclidean distance to k weight vectors
e	Exponential
FPs	False positive value
$f(m,n)$	Original image intensity
GT	Ground truth image
G_x, G_y, G_z	Gradient of pixel *(i,j,k)*
$g(m,n)$	Image display value
$g(x)$	Intensity of original image
$g(y)$	Intensity of pixel in region of interest
HU	Hounsfield units
I_{max}	Maximum intensity of the original image
$I_{(x,y)}$	Pixel intensity at *(x,y)*
i, j, k	Iteration number, Index
$\vec{n}$	Normal vector
p	Coordinate of marked pixels, Percentage of overlapping area
PM	Percent Match
R_x, R_y, R_k	Rotation matrix about $x,y,$ and k axis

LIST OF ABBREVIATION (cont.)

S_1, S_2	Distances from object
$S(t)$	b-splines curve segment
TPs	True positive value
u	Length of mesh
V	Cube corner value
v_{cubic}	Volume of cubic
$v_{cylinder}$	Volume of cylinder
$v_{ellipsoid}$	Volume of ellipsoid
$W(t)$	Weight vectors
x , y, z	Pixel index
$\Delta x, \Delta y, \Delta z$	length of the cube in $x,y,$ and k direction
y_{SOM}	Intensity of representatiov image
α	Angle of light vectors
$\alpha(t)$	Monotonically decreasing functions of time
$\theta(t)$	Monotonically decreasing functions of distant
$\sigma(t)$	Monotonically decreasing functions of iteration
$\tilde{\sigma}$	Growing threshold
$\delta(x)$	Intensity difference
λ	Time constant

CHAPTER I
INTRODUCTION

1.1 Problem Statement

Cancer is a disease that highly affects quality of life of people and mortality rate. According to the global burden of disease published by world health organization (WHO) in 2004, cancer is ranked in the 3rd leading cause of dead in men and women. The actual causes and its progressive are still imprecisely expressed. However, some factors are suspicious to be the causes such as genetics, food, toxicity, viral infection, or ageing because they can impair the cell cycle and cause the uncontrollable cell reproduction mechanism [1].

Nasopharyngeal carcinoma (NPC) focused in this study is one type of head and neck cancers. In 2004, it is the second most common cancer frequently found in Southeast Asia including Thailand, Malaysia etc. [2]. It is also in the 7th most common cancer discovered in the other parts of the world. Signs and symptoms of NPC are not obviously observed because they are similar to the flu. Most of the patients disregard their symptoms until either throat bleeding or throat swelling arise. Therefore, NPC is usually detected when it is in the severe stage. In clinical pathology, physicians have to use a specific medical device, called the Laryngoscopy in detecting the tumor. The Laryngoscopy normally examines the tumor through a camera attached inside. It can cut a piece of suspicious tissue to do the biopsy. However, cancer invasion cannot be accurately identified. In general, CT and MR images of a patient are used to provide necessary information in cancer management. The information includes the common site, cell growth and lymphatic invasion patterns. MR images normally provide NPC regions clearer than CT images. However, it is costly and not widely used in Thailand. In this thesis, CT images are mainly focused. To gain useful information from CT images, physicians have to correctly identify the NPC regions in each image. Because of the tumor image intensity in the CT images are close to that of the normal tissue,

physicians have to cautiously select the NPC region. In case that there are many CT slices, manual selection is prone to error and it is the tedious task.

This research aims to develop software for semi-automatic image segmentation and 3D visualization of NPC from CT images. A segmentation technique based on the self organizing map (SOM) is proposed in order to extract the tumor region from the CT images. Initial tumor pixels, called seed points, must be specified. Information from the seed points is used to determine the tumor extent in a CT image. After the tumor regions are selected from the images, 3D model of the tumor is constructed and presented in the virtual skull. This model is useful for physicians in order to diagnose and plan the treatment. Useful information such as common site, cell growth and lymphatic invasion patterns can be easily observed. The 3D model can be used for surgical guidance or radiotherapy planning. In addition, physicians can compare the 3D models of pre and post-treatments in order to evaluate the treatment efficiency. The performance of this segmentation algorithm is measured by comparing among area of tumor region which manually identified by experienced radiologists, and the quality of 3D reconstruction is also compared to the 2D image which created parametric equations.

1.2 Thesis Objectives

1.2.1 To propose an adaptive self organizing map technique for CT images segmentation. The performance of segmentation should be superior to at least two previously proposed techniques.

1.2.2 To develop 3D NPC visualization algorithm from CT images in which radiologists can manually select the tumor regions from CT images.

1.2.3 To investigate common site and growth pattern of NPC in any stage.

1.3 Thesis Scopes

1.3.1 Develop software that is easy to manually select NPC regions for radiologists.

1.3.2 Semi-automatically segment NPC tissue from CT images.

1.3.3 Automatically construct 3D NPC model from CT images

1.3.4 Display the tumor model onto the virtual skull or other anatomical landmarks.

1.3.5 Compare the constructed model with other 3D model reconstruction techniques.

1.3.6 Examine common site and growth pattern of NPC in any stage from the constructed model.

1.4 Expected Results

1.4.1 Obtain new adaptive self organizing map technique for CT images segmentation. The performance of segmentation should be superior to at least two previously proposed techniques.

1.4.2 Obtain 3D NPC visualization algorithm from CT images in which radiologists can manually select the tumor regions from CT images.

1.4.3 Obtain investigation software for observe common site and growth pattern of NPC in any stage.

CHAPTER II
THEORETICAL BACKGROUND AND RELATED RESEARCH

Overview of nasopharyngeal carcinoma, medical image processing, segmentation techniques, 3D reconstruction, and related research are presented in this chapter.

2.1 Nasopharyngeal Carcinoma: Anatomy

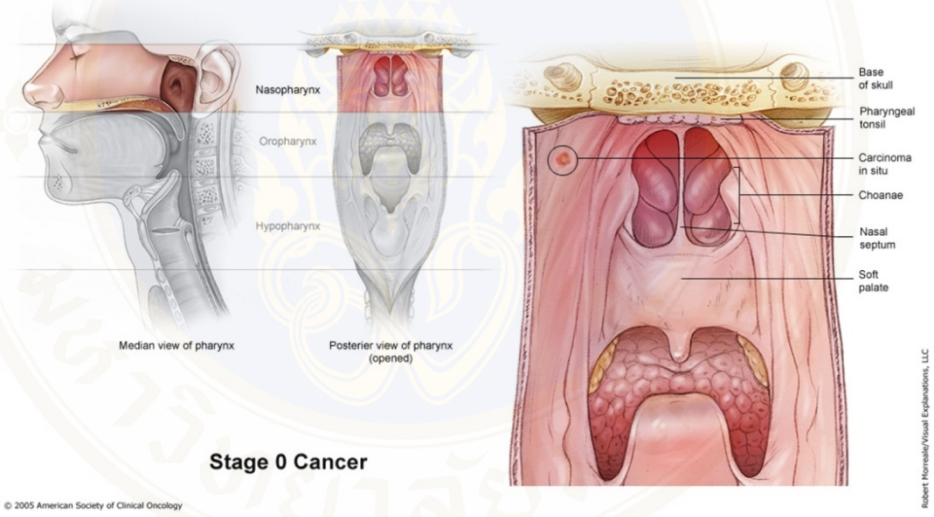

Figure 2.1 Anatomy of nasopharynx [3]

Nasopharynx is a part of pharynx, behind the nasal cavity and above the oropharynx as seen in figure 1. Its boundary is connected with various parts as described below:

- Anterior: posterior choanae.
- Inferior: oropharynx.
- Superior: basisphenoid and basioccipital bone.
- Posterior: longus colli and capitis muscles which are in front of C1 and C2 cervical vertebras.
- Lateral: open end of Eustachian tube and Rosenmuller's fossa.

2.2 Treatment

Conventional treatment of NPC patients is chemotherapy, radiotherapy, surgery, or combinations of them. For treatment planning, tumor information is necessary and can be easily obtained through CT images. The information includes size, location, and invasion etc.

2.3 DICOM file format

Digital Imaging and Communications in Medicine (DICOM) is a standard file format for medical images [4]. It is used in Picture Archiving and Communication System (PACS) in order to transfer images between computers. This format consists of two parts, i.e., header and image parts. The header contains file information and patient data. The image part stores image data in the hex format. For CT images, standard size of image is 512*512 pixels and it is often stored as 2 bytes per pixel. Each pixel of a CT image is normally represented in Hounsfield units HU [5]. For this representation, water is set to zero while air is -1000 HU. Before manipulating a CT image, the image in HU unit must be converted into pixel value as shown in Eq. (1)

$$pixel\_value = \frac{HU - interception}{slope} \quad (1)$$

where interception and slope are parameters stored in the DICOM header file with the rescale interception and rescale slope tag-names respectively.

In general, it is normal to obtain CT images from different views or acquisitions [6], such as pre- and post-contrast CT scans. Each view or acquisition is called a series. In a DICOM series, it contains the number of CT slices. Each slice is stored in a DICOM file format as presented above. Patient data, the number of series, series name, the number of images in each series, and image file name are provided in a log file, named DICOMDIR. In order to manipuate a CT image, DICOMDIR must be initially explored. The required series is then selected. After that, a particular CT image in the selected series can be proceeded.

2.4 Basic Image Processing Techniques

In this section, basic operations of image processing used in this thesis are presented.

2.4.1 Contrast adjustment

In order to clearly view an image, brightness and contrast should be appropriately adjusted. There are various contrast adjustment techniques, such as histogram equalization and contrast stretching etc. In this subsection, linear contrast stretching technique is presented. Contrast of an image is linearly scaled by

$$g(m,n) = \begin{cases} 0 & ; f(m,n) < a \\ \frac{I_{max}}{b-a}(f(m,n)-a) & ; a \le f(m,n) \le b \\ I_{max} & ; f(m,n) > b \end{cases} \quad (2)$$

where $g(m,n)$ is image display value at the pixel (m,n). $f(m,n)$ is the original image intensity. Terms *a* and *b* represent minimum and maximum intensity values of user-specified range. I_{max} presents the maximum intensity of the original image. Pixels having intensities lower than a will be displayed as dark pixels (zero display intensity). On the contrary, intensities above *b* will be presented by the brightest pixels (I_{max}). Figure 2.2 shows linear transformation from image intensities to display intensities. Example of applying linear contrast stretching to a CT image is shown in Figure 2.3.

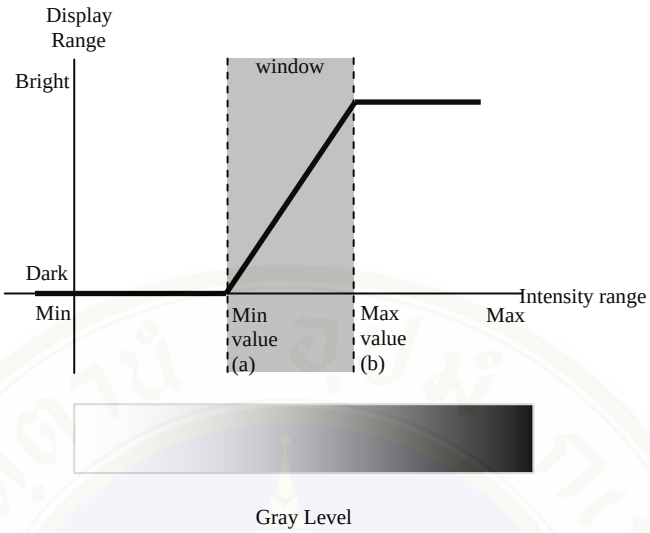

Figure 2.2 Linear contrast stretching

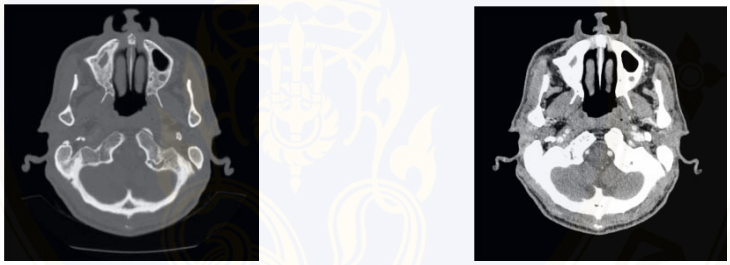

a) **b)**

Figure 2.3 Example of applying linear contrast stretching
a) Original image with the intensity range, [0 I_{max}] = [0 2600]
b) Adjusted image with user-specified range, [a b] = [950 1250]

Figure 2.3a) shows an original CT image having image intensities between 0 and 2600. After linear contrast stretching is applied, the image can be clearly visualized as seen in Figure 2.3b).

2.4.2 Zoom in and zoom out

Zoom is a method of adjusting angle of view while maintaining the aspect ratio as same as the original image [7]. It is involved with the image interpolation. In general, there exist 2 zooming ways, i.e., zoom in and zoom out. Zoom in is to reduce the angle of view. The region of interest is thus magnified. On the contrary, zoom out is the increasing approach. This results in the smaller image appearance. The zoom in

technique works as follows. Initially, each pixel of the image is surrounded by zero pixels added to magnify the image size as shown in Figure 2.4. In the figure, the original and the padded images are presented.

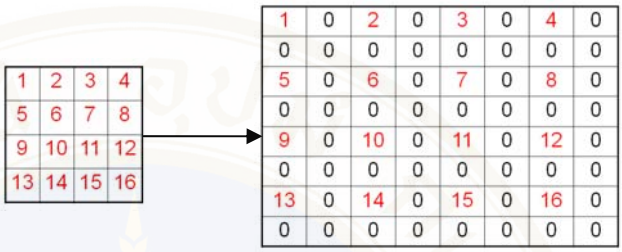

Figure 2.4 Original and padded images

The padded image contains discontinuous image intensities. Image interpolation technique is thus applied in order to provide continuous image intensities. In this thesis, bicubic convolution interpolation is employed in order to efficiently maintain the image content [8]. Figures 2.5 and 2.6 show an example of bicubic kernel and the interpolated image.

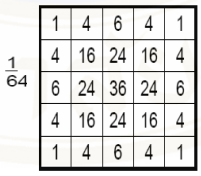

Figure 2.5 Bicubic interpolation kernel

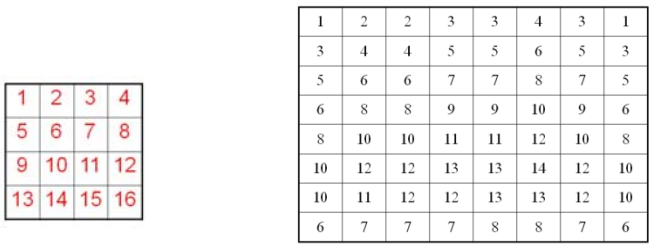

a) **b)**

Figure 2.6 a) Original image, b) Interpolated image

2.4.3 Image Rotation

Image rotation is used to rotate an image at arbitrary angle in any direction. It is used to visualize sagittal and coronal planes from the original images presented in the transverse plane. Figure 2.7 shows cross sectional area of human body in different planes. Medical doctor uses image information from these planes in diagnosis and treatment. In order to represent CT images in these planes, image rotation takes an important role. Initially, all CT slices in a selected series are aligned in sequence as shown in Figure 2.8. By rotating the aligned images 90 degrees with respect to the y axis, images in the coronal view can be obtained. In the similar manner, by rotating 90 degrees with respect to the x axis, images in the sagittal view can be gained.

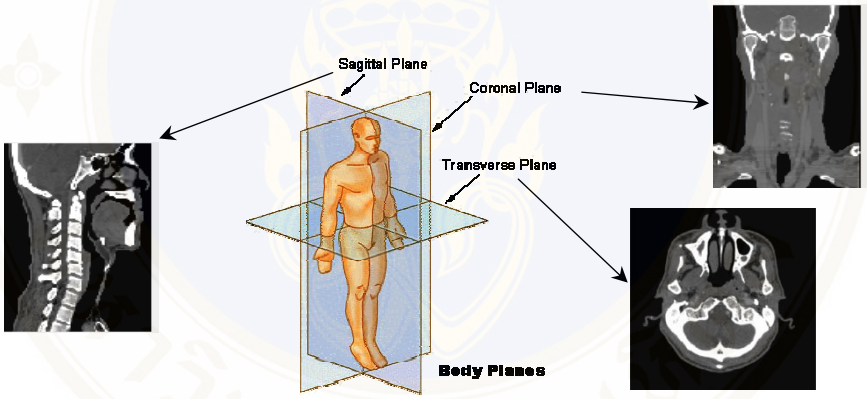

Figure 2.7 CT images in different planes [9].

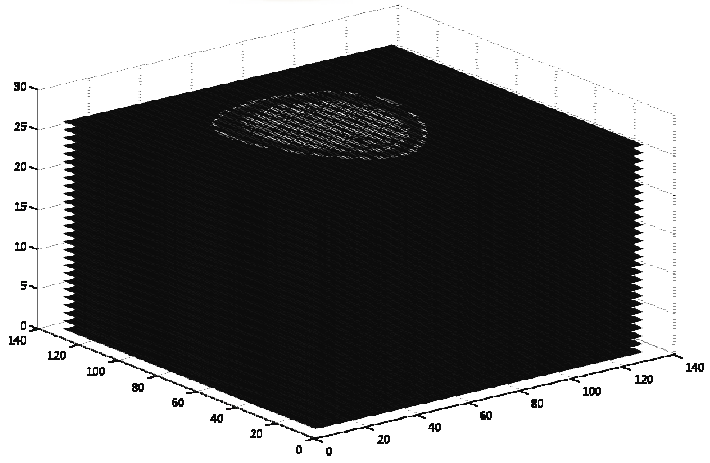

Figure 2.8 Aligned CT series

To rotate an array of aligned CT images with respect to a certain axis, rotation matrix is used. Rotation matrix about x axis is given by

$$R_x = \begin{bmatrix} 1 & 0 & 0 \\ 0 & cos\theta & -sin\theta \\ 0 & sin\theta & cos\theta \end{bmatrix} \quad . \quad (3)$$

The rotation matrix about y axis is presented as

$$R_y = \begin{bmatrix} cos\theta & 0 & sin\theta \\ 0 & 1 & 0 \\ sin\theta & 0 & cos\theta \end{bmatrix} \quad . \quad (4)$$

In order to rotate the image, new coordinate of the rotated image is derived from

$$\begin{bmatrix} x' \\ y' \\ z' \end{bmatrix} = R_k \begin{bmatrix} x \\ y \\ z \end{bmatrix} \quad , \quad (5)$$

where R_k is the rotation matrix about k axis.

2.4.4 Morphological Operations

In order to extract shape, boundary, skeleton of a binary image, morphological operations are employed. The operations used in this thesis include dilation and erosion. Image dilation and erosion are techniques for enlarging and reducing boundary regions of the foreground pixels respectively [10]. Initially, structural element for the dilation and erosion must be specified. For the dilation technique, the structure element is moved onto the binary image pixel-by-pixel. If the central point of the structural element coincides with the white pixel of the image, intensity of the pixels locating in the same position of white structure element pixels will be changed into one as seen in Figure 2.9. For the erosion technique, the structural element is also moved across the image. When the central point and its neighboring white pixels locate on the white pixels of the image, the pixel in the same location of the central point is marked. After all pixels in the image are considered, all marked

pixels are maintained as the white pixel. The other unmarked pixels are converted into the black pixels. Figure 2.10 shows an example of the image erosion.

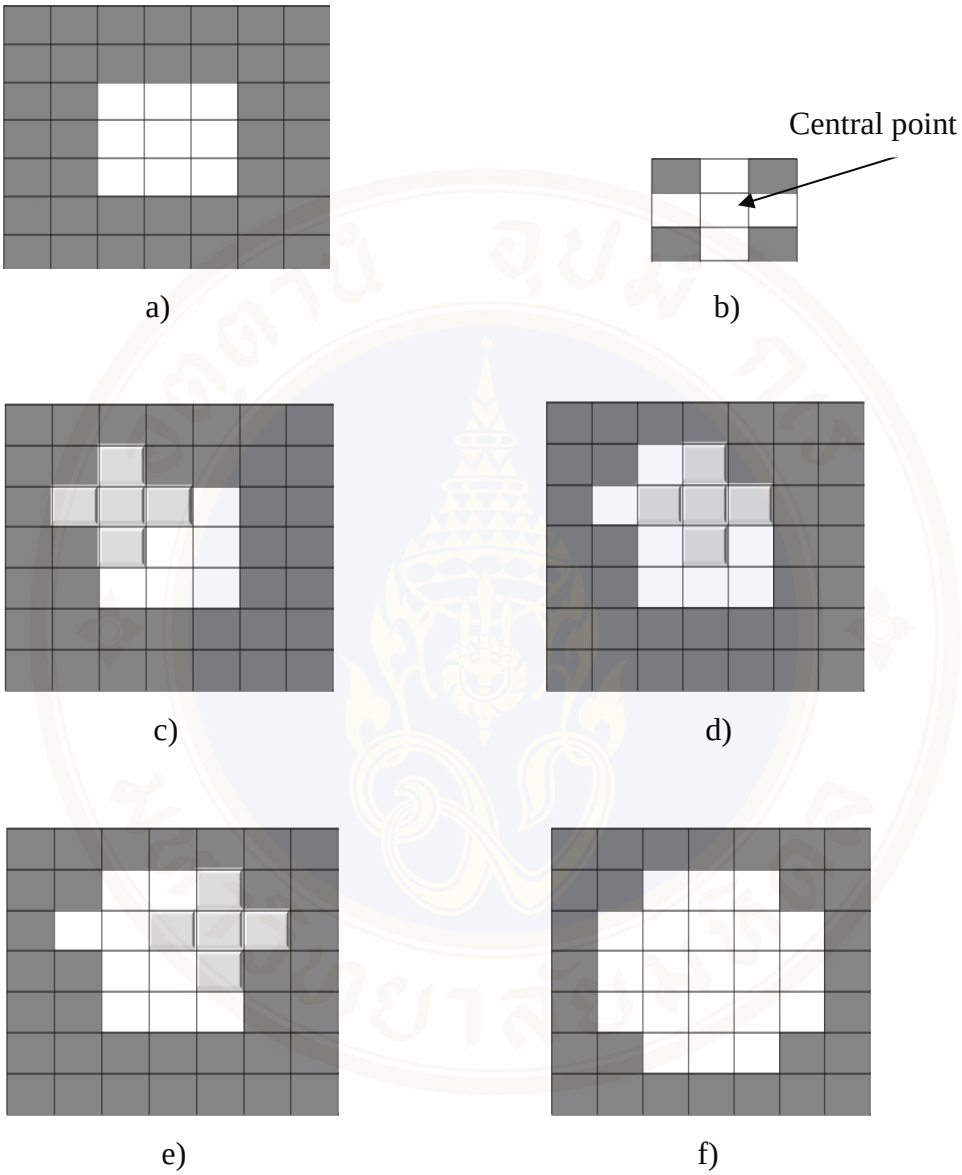

Figure 2.9 Example of image dilation
a) Original image
b) Structural element
c) 1st expanded foreground pixel
d) 2nd expanded foreground pixel
e) 3rd expanded foreground pixel
f) Dilated image

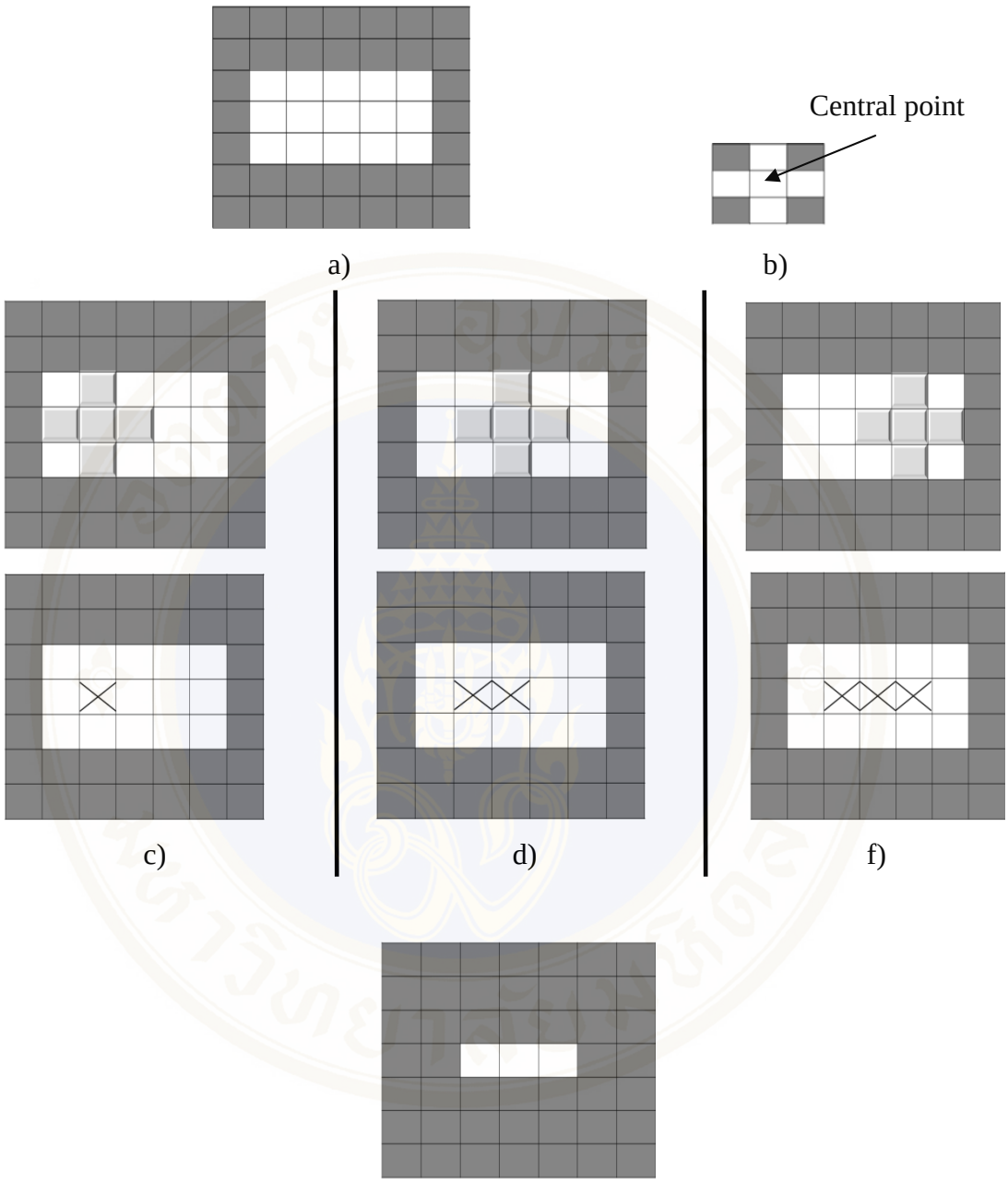

Figure 2.10 Example of image erosion

a) Original image

b) Structural element

c) 1st marked pixel

d) 2nd marked pixel

e) 3rd marked pixel

f) Eroded image

2.4.5 Tumor image segmentation

To provide efficient diagnosis and treatment of NPC, tumor information from CT images is utilized. The information includes location, size, invasion pattern etc. For a patient, there may be 20-100 CT slices must be taken into account. Physicians have to carefully delineate tumor region in a CT image slice-by-slice. This is cumbersome and prone to error particularly when the number of patients is huge. Medical image segmentation technique can relieve this burden. In general, the image segmentation techniques can be categorized into 3 main approaches. They are 1.) Intensity based approach 2.) Pattern based approach, and 3.) Deformable model approach.

Intensity based approach uses intensity information or its gradient information to separate a tumor region from other tissues in an image. The underlying idea of this approach is that an object in an image should contain similar intensities. The techniques in this approach are thresholding [11]-[13], region growing etc. Thresholding technique segments an object by checking whether the image intensities are within a predefined range. Region growing method is proposed by Adams and Bischof [14]. Initially, a seed representing tumor pixel must be specified. Its intensity is used to determine a range of tumor image intensities. This algorithm starts by searching all nearby pixels of the initial seed. If their image intensities are within the range, the pixels will be included as tumor pixels. Searching is continuously performed until there is no nearby tumor pixel. Though this approach is relatively simple, it is sensitive to image intensities and noises. To apply this approach efficiently, some pre-processing techniques, such as contrast adjustment, image normalization etc. are required.

Pattern based approach uses a pattern of an object of interest in segmentation. The pattern can be gained from supervised and unsupervised learning methods. Supervised learning methods learn to classify tumor and non-tumor pixel from a training dataset. The dataset composes of tumor and non-tumor features that may be extracted from the intensity, location, and size of the tumor etc. An example of using this technique in segmentation is Zhou's work [15].Support vector machine [16] was employed to segment NPC. Zhou creates feature space and projects all training data onto the space. Basic idea of this technique is that data in the same class should have

similar features and be projected onto analogous location. Support vector machine thus can easily classify tumor and non-tumor regions. A major drawback of the supervised learning methods is that they require appropriate training examples. Inappropriate examples may cause undesired segmentation results. The training dataset must be carefully prepared. Moreover, accurate segmentation can be achieved when the number of training data is large. Computational resources are thus costly.

Unsupervised learning methods do not require the training examples. They use the image feature in clustering. Each image is clustered into several groups. For tumor segmentation, the groups may be tumor and non-tumor groups. Murugavalli and Rajamani [17] applied fuzzy c-mean clustering for brain tumor segmentation from MR images. Initially, the number of classes was specified. Mean of each class was adapted from the training data. After the training, all mean values were used in the segmentation. Each pixel is clustered into a class that has the mean value closest to the pixel's intensity. These techniques are relative simple in which training examples are not required. They are also easily adapted to new segmentation criterion.

The last approach is based on deformable model. It concerns the physical appearance of tumor in an image. The appearance includes shape or contour. Active contour or snake is a famous technique in this approach. Dubey [18] applied it to segment the brain tumor in MR images. Initial curve was placed in the image prior to the segmentation. Virtual internal and external forces were formulated to exert the contour. These forces were adjusted the curve until it fit with the tumor region. This approach is effective when the contour of the object of interest is prominent. For the object which its contour is not obviously observed, this technique performs poorly. Moreover, the technique require initial curve which should be placed the closest possible to the segmented object.

2.4.6 Performance evaluation in image segmentation

In order to evaluate the segmented region, in general, Corresponding Ratio (CR) and Percent Match (PM) are used. Initially, standard ground truth images (*GT*) must be provided. The segmented region is compared with the ground truth images. The corresponding ratio and perfect match are given by

$$CR = \frac{TPs - 0.5 * FPs}{GT} \quad (6)$$

$$PM = \frac{TPs}{GT} * 100 \quad (7)$$

where *TPs* is true positive value representing the number of segmented pixels that coincide with a standard ground truth image. *FPs* presents false positive value. It represents the number of segmented pixels that do not locate in the standard ground truth image. Both CR and PM can be used to measure the segmentation performances. Higher CR value means that the segmented result contains more true positive value while less false positive value. Greater PM value indicates that the result has higher true positive value. The perfect segmentation is obtained when CR equal to 1 and PM equal to 100%.

2.5 3D Visualization

In order to visualize a 3D model from multiple CT slices, in general, there are 2 main rendering methods, i.e., surface rendering and volume rendering. Surface rendering creates a 3D model by placing polygons in appropriate locations. Volume rendoring, on the other hand, create artificial voxels from image pixels..

For surface rendoring, surface of a 3D object is generated from 2D contour of the object in each slice. The contour can be determined from the thresholding Figure 2.11b presents the contours extracted by the thresholding method. After that, the contours are aligned in sequence as shown in Figure 2.11c.

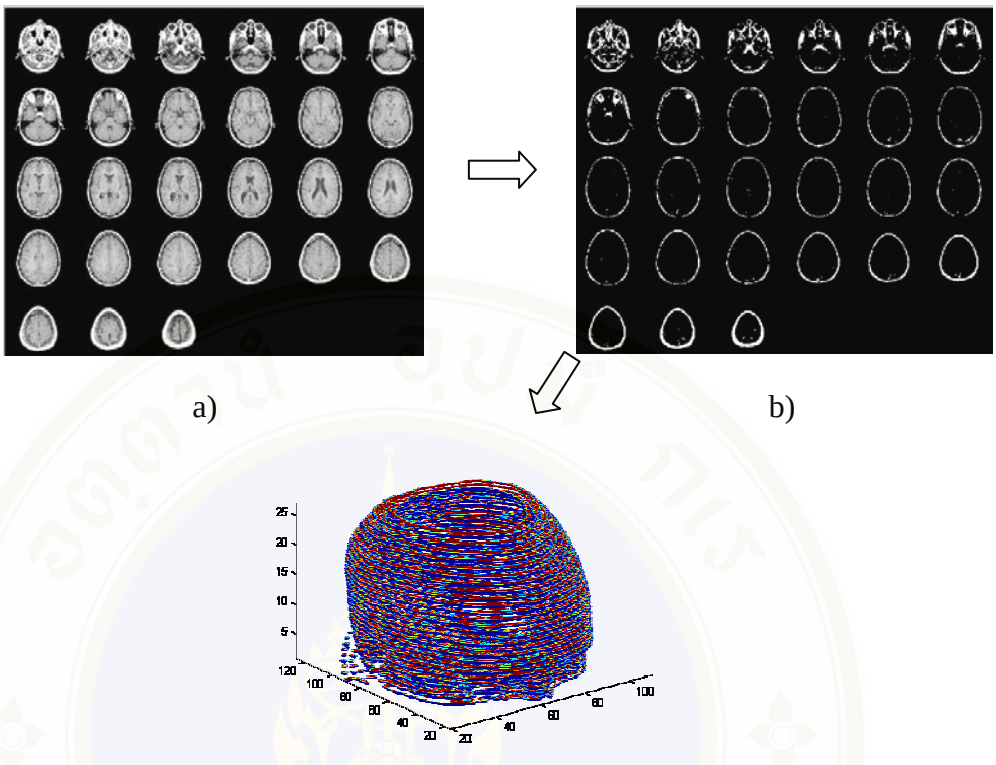

Figure 2.11 Contour extraction
a) CT slices
b) Extracted contours using the thresholding method
c) Aligned coutours

The aligned contours are employed to determine coordinate to place the polygon in 3D scene. The coordinate is called vertex. In order to determine the vertex from the contours, marching cube technique is generally used. There are 2 major steps to calculate the vertrics using marching cube. First, A logical cube is created and moved along the pixel coordinates between two neighboring contour slices as shown in Figure 2.12. For each marching, the vertex is created according to the matched pattern of corner pixels in the cube as shown in Figure 2.13. In this figure, the circular dot represents a logical 1. Once the moved cube meets logical corners similar to one of the patterns defined in Figure 2.13, polygon mesh of that pattern is drawn. All meshes from the 3D surface.

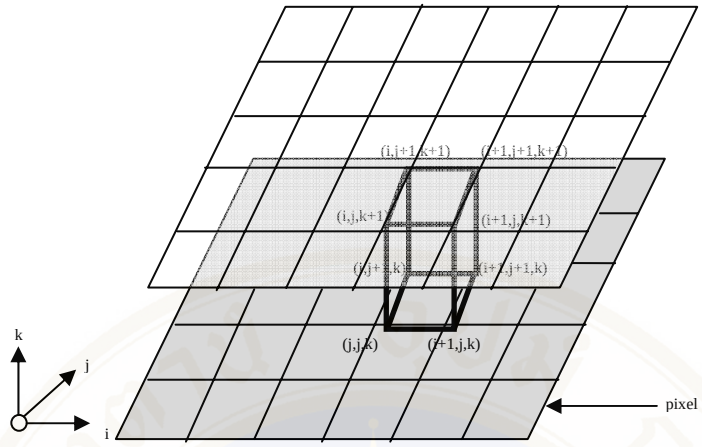

Figure 2.12 A graphical image presents Marching cube process.

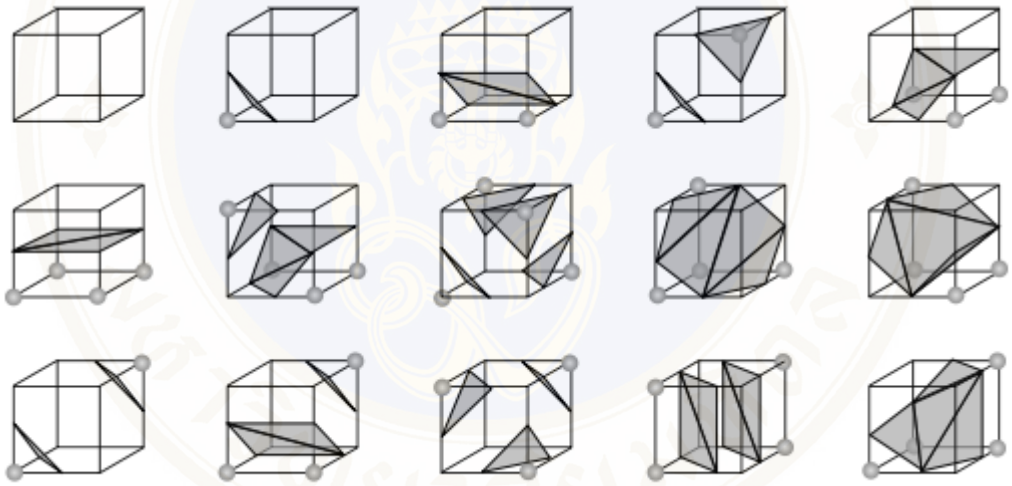

Figure 2.13 Configuration and amount of polygons of 15 unique patterns.[19]

In general, trigon or polygon mesh is used for creating a rigid model. The trigon is the simplest pattern of polygon and smooth curve can be gained from the trigon mesh without bending or distorting its shape as presented in Figure 2.14.

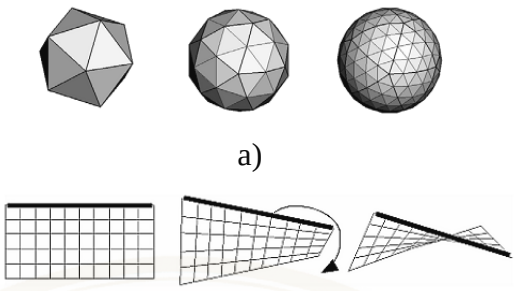

a)

b)

Figure 2.14 a) Circles created from trigons, smaller trigon creates smoother surfece. b) Tetragon will be distorted when it is bended to create curved surface.

Finally, The normal vector of each vertex is calculated. This normal vector is essential for rendering in order to provide smooth light effect on low-polygon surface. Figure 2.15 shows Gouraud shading which is a way to simulate different effects of light and color across the surface of an object.

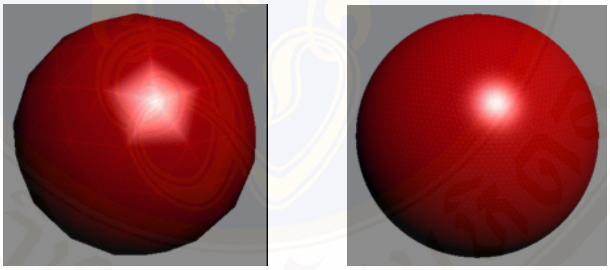

a) Gouraud shading off b) Gouraud shading on

Figure 2.15 Rendering a sphere with Gouraud shading [20]

This normal value can be specified by normal gradient of the surface. The geadient is the derivative of the density function of pixel in a vertex as given by

$$G_x(i,j,k) = \frac{D(i+1,j,k)-D(i-1,j,k)}{\Delta x} \quad (8)$$

$$G_y(i,j,k) = \frac{D(i,j+1,k)-D(i,j-1,k)}{\Delta y} \quad (9)$$

$$G_z(i,j,k) = \frac{D(i,j,k+1)-D(i,j,k-1)}{\Delta z} \quad (10)$$

Where G_x, G_y, G_z are gradient of pixel (i,j,k) in x,y,z directions. D(i,j,k) is the derivative of density function of pixel (i,j,k). $\Delta x, \Delta y, \Delta z$ are length of the cube in each direction. The normal vector $\vec{n}$ can be estimated from linearly interpolation of the gradient at the point of interest as pressented in Figure 2.16. Example of surface rendering using marching cube algorithm can be shown in Figure 2.17.

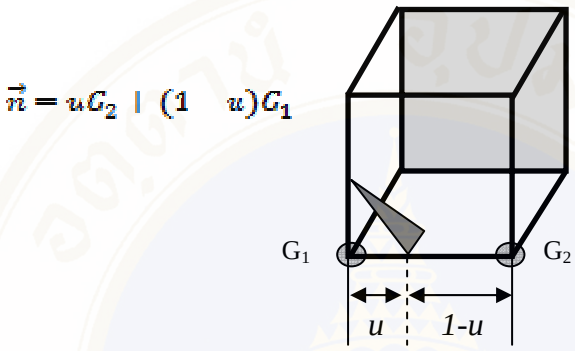

Figure 2.16 Normal vector calculation.

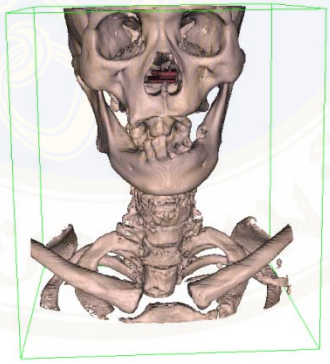

Figure 2.17 Example of surface rendering of human head from marching cube algorithm

Volume rendering creates array of voxels from pixels.[21] Voxel is a volume element. In this study, volume ray casting technique is employed. The technique creates high quality volume model by adding intermediate points between 2D slices in order to fulfill gap between the slices. Trilinear interpolation given by Eq. (11) is used to interpolate value of an intermediate point (x,y,z). Figure 2.18 shows a unit cube.

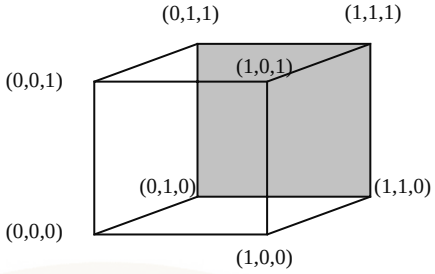

Figure 2.18 Unit cube

The intermediate point of the unit cube can be determined from

$$V_{xyz} = V_{000}(1-x)(1-y)(1-z) + V_{100}x(1-y)(1-z) + V_{010}(1-x)y(1-z) \quad (11)$$
$$z + V_{001}(1-x)(1-y)z + V_{101}x(1-y)z + V_{011}(1-x)yz$$
$$+ V_{110}\,x\,y\,(-z) + V_{111}\,x\,y\,z$$

where the cube corners are defined as V_{000} ,V_{001} ,V_{010} , …, V_{111} reepectively. The process of volume ray casting consists of 4 steps as presented below.

1. Ray casting. Assume that all 2D slices are aligned in sequence in front of the monitor in θ angle as presented in Figure 2.19. Observer views these slices through the monitor. Line of sight, or ray is directly projected on to the pixels of the slices. All pixels (called casted pixels) that the ray passes are taken into account and they are used for the volume interpolating process.

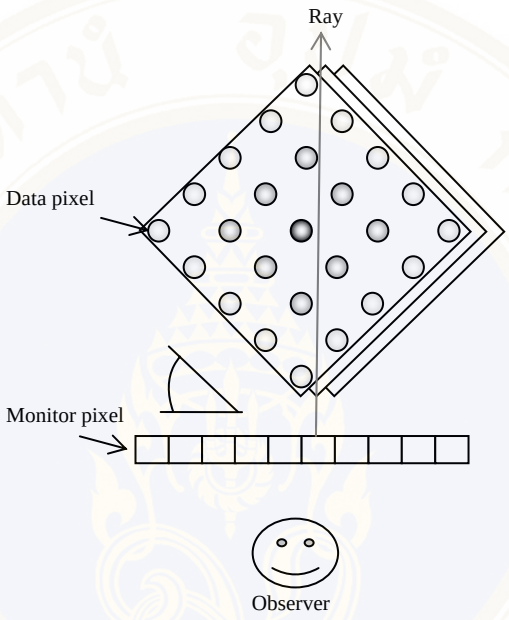

Figure 2.19 A concept of ray casting process.

2. Sampling. Gap between slices that the ray passes are fulfulled with voxels as shown in Figure 2.20. Each voxel has the same size and its corresponding intensitiy values are determined from trilinear interpolation.

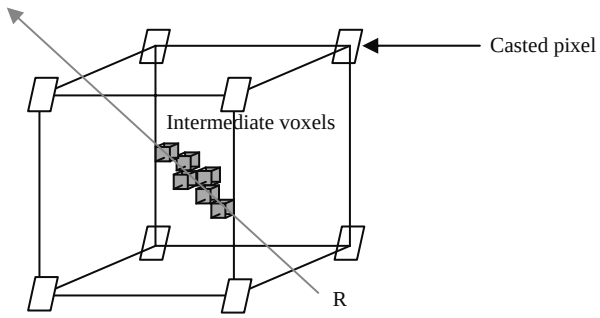

Figure 2.20 Voxles placed along the ray line

3. Shading. The light source is predefined in the 3D scene. This process calculates the light effect on each voxel using intensity and initial parameters including color, ambient, and opacity. Figure 2.21 presents the shading process.

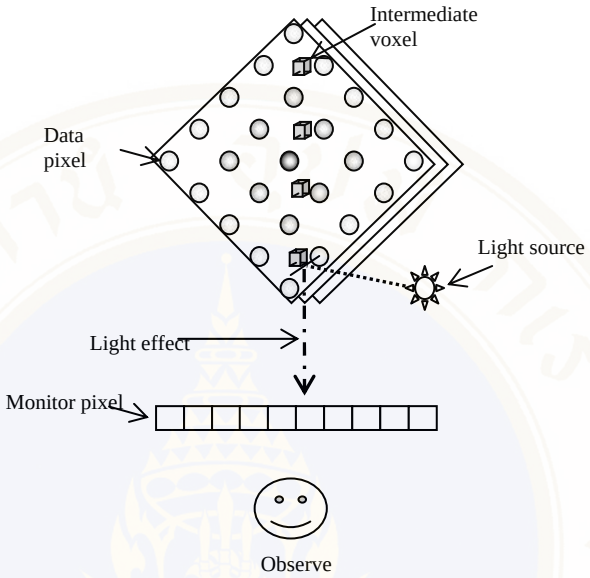

Figure 2.21 The shading process

4. Composition. The ray is projected back-to-front in oder to accumulate sum of shading results along the ray line. The accumulated result is presented on the monitor pixel. Some visualization effects may be added here, i.e., distortion. Figure 2.22 presents composition process. Example of volume ray casting is shown in Figure 2.23.

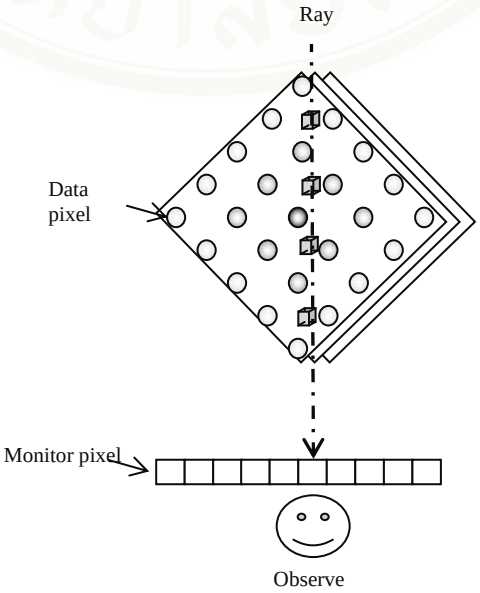

Figure 2.22 Composition process

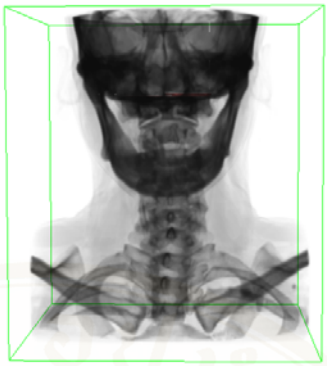

Figure 2.23 Example of volume ray casting.

2.5.1Tumor volume validation

In order to ensure that the tumor volume determined from the 3D model constructed is accurate, virtual geometry models are created and used in the validation. The virtual models include cubic, cylinder, and ellipsoid. Their volume can be determined from

$$v_{cubic} = x * y * z \quad (12)$$

$$v_{cylinder} = \pi r^2 h \quad (13)$$

$$v_{ellipsoid} = \frac{4}{3}\pi * x * y * z \quad (14)$$

where V_{cubic}, $V_{cylinder}$, $V_{ellipsoid}$ are the volume of cubic, cylinder and ellipsoid respectively. x,y,z are the distance along x,y,z axes, r and h are the radius and height of cylinder respectively. These models are sliced into multiple 2D images and reconstructed into 3D models through the volume rendering technique presented previously. Volume of each model is computed from the number of voxels and compared with its geometry.

2.6 Software Development

In this section, the developed software is presented. The software is composed of 4 main functions. They are 1.) DICOM image acquisition 2.) Image display 3.) Image segmentation, and 4.) 3D reconstruction. Each function and sub-functions can be presented below.

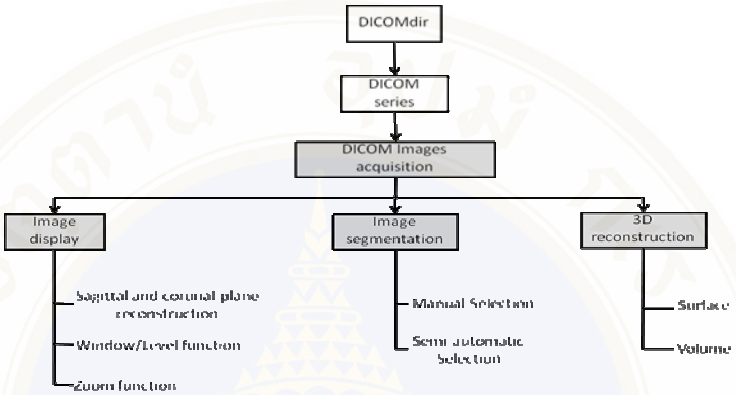

Figure 2.24 Overall functions of the software

2.6.1 DICOM image acquisition.

Normally, CT images are stored in DICOM file version 3.0. Patient's information and image data are retrieved from DICOMDIR which contains information compatible with DICOM header. All image series are displayed through designed Graphical User Interface (GUI) to allow selecting a DICOM series. Patient's information and acquisition technique are presented shortly and used as name of the DICOM series. An example of the DICOM image acquisition window can be presented in Figure 2.25.

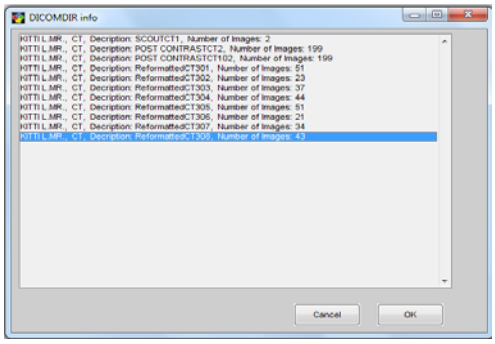

Figure 2.25 GUI for DICOM series selection

2.6.2 Image display

The developed software can visualize each CT image in 3 plains. Layout of the software is shown in Figure 2.26. Main window is in the middle of the screen. It presents the transverse view of the image. Sagittal, and coronal views are displayed on the windows on the right side. The scrollbar below each window allows user to navigate the CT images in its series. There are 2 sub functions supporting the image display, i.e., contrast adjustment and zoom function. With the contrast adjustment, user can adjust the contrast and brightness of the image presented on the screen. Zoom function allows magnification of the image. In this software, user can specify up to 6x zoom power.

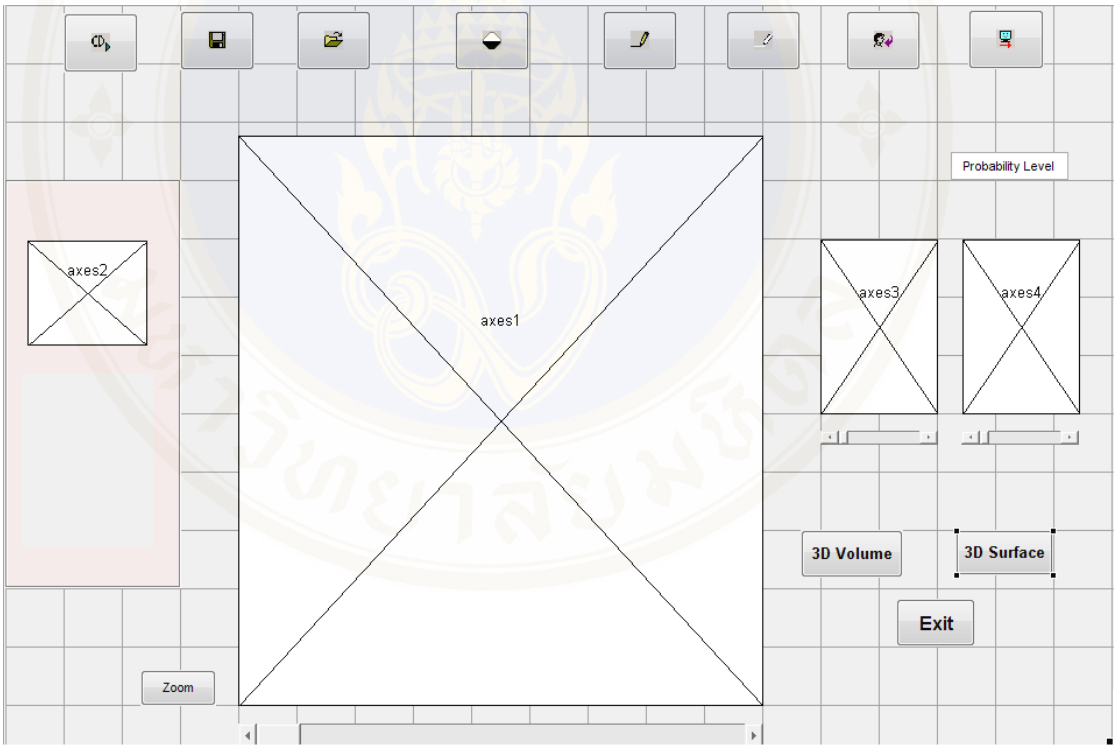

Figure 2.26 Layout of the software.

2.6.3 Image segmentation

This function consists 2 sub-functions; manual segmentation and semi-automatic image segmentation. Manual segmentation allows user to delineate tumor region manually. Initially, users have to specify tumor pixels on the image. The interpolation method is employed to draw curve among the selected points. In this software, cubic b-spline interpolation is used because it does not encounter with Runge's phenomenon (peak of the interpolated curve overshoots when high order polynomial function is assigned) [22]. The b-spline curve is calculated from solving Eq. (15). Example of the cubic b-spline curve is shown in Figure 2.27.

Figure 2.27 Example of cubic b-spline curve.

$$S_i(t) = [t^3 \;\; t^2 \; t \;\; 1]\frac{1}{6}\begin{bmatrix} -1 & 3 & -3 & 1 \\ 3 & -6 & 3 & 0 \\ -3 & 0 & 3 & 0 \\ 1 & 4 & 1 & 0 \end{bmatrix}\begin{bmatrix} P_{i-1} \\ P_i \\ P_{i+1} \\ P_{i+2} \end{bmatrix} \quad for\ t \in [0,1] \quad , \qquad (15)$$

where $S(i)$ is the b-splines curve segment, P is the coordinate of marked pixels, so called the control point. i is the control point index, and t represents intermediate point between the marked pixels. It is set as 100 points between two marks.

Another sub-function is semi-automatic image segmentation. User can segment the tumor region by selecting an initial tumor pixel, called seed point. Information from the seed point is used for determining the tumor region. One seed can create only one region. User can choose more than one seed for segmenting multiple regions. This function is composed of 4 main steps. Initially, location of the CT image of interest is identified. This is because common site of NPC is different in each location. The images are normalized in order to adjust their scale to be in the same range. Representatives of NPC images constructed by Self Organizing Map (SOM) are used in the segmentation. The representative image that is the most similar

to a CT image of interest is taken into consideration. The specified seed is marked on this representative. Region growing is then applied. Locations of pixels which are similar to the marked seed are collected. These locations are used for retrieving intensities of pixels on the CT image of interest. Mode of these intensities is determined. Region growing on the CT image is performed at the location of the initial seed. Mode intensity is used in place of seed's intensity. The segmented region represents area of NPC. All segmentation steps are summarized as shown in Figure 2.28.

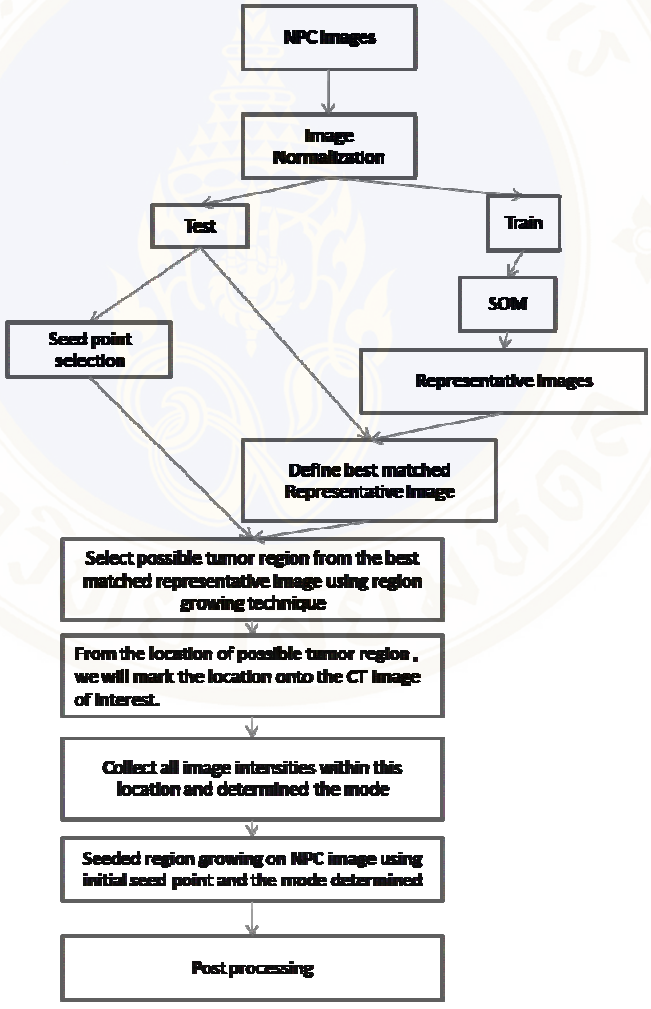

Figure 2.28 Proposed semi-automatic segmentation technique

1. CT image location identification

This process classifies a CT image into one of three groups according to its location on the human skull. These groups represent different parts of the skull, i.e., above orbital sockets, between the orbital sockets and hard palate, and below the hard palate as shown in Figure 2.29. Because the common site of NPC is different in each location, it is necessary to identify which group the CT image belongs to. Bone structure is used in the classification because it is no different among patients.

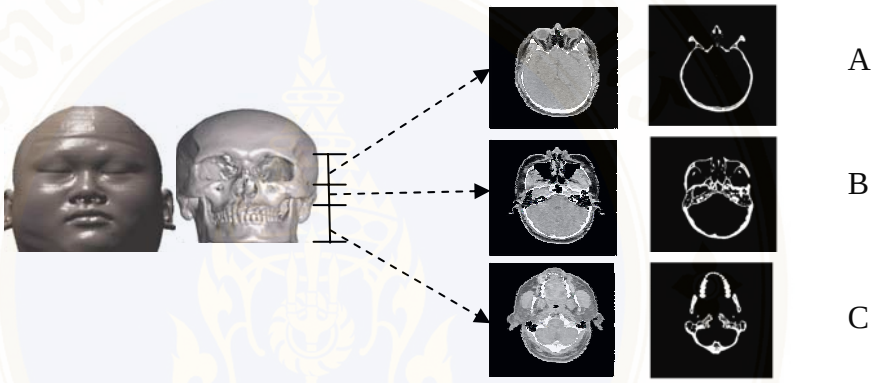

Figure 2.29 Classification of human skull into three groups
A) Above orbital sockets
B) Between orbital sockets and hard palate
C) Below hard palate

In order to identify location of the CT image, dimension of skull inside the images is initially normalized. This is because the apparent size of the skull may be different in each image. Difference in size occurs from adjusting the field of view (FOV) during image acquisition process. In general, FOV of a CT image can be presented by a circular region as shown in Figure 2.30. Inside this region, skull and other organs exist.

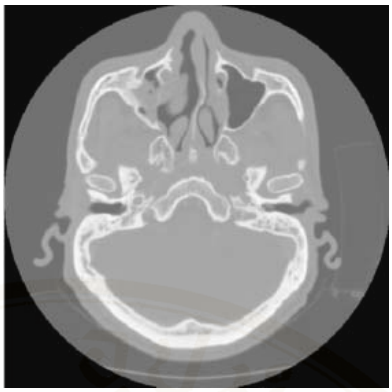

Figure 2.30 An example of FOV in a CT image

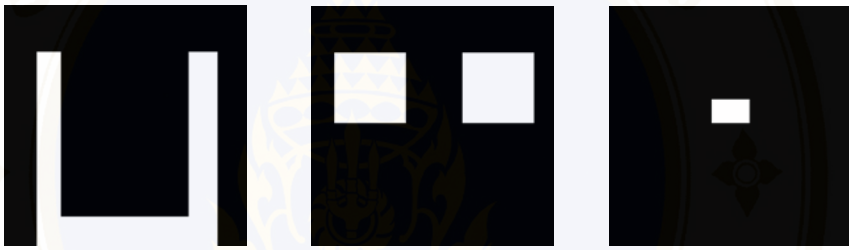

a) Template 1 b) Template 2 c) Template 3

Figure 2.31 Templates for classify the image types.

Three different templates presented in Figure 2.31 are generated. Bone structure in the CT image is then extracted using the thresholding technique and compared with each template as shown in Figure 2.32. Percentage of overlapping area is computed by

$$P = \frac{\sum_1^m \sum_1^n \{ I_{template}(x,y) \wedge I_{skull}(x,y) \}}{\sum_1^m \sum_1^n (I_{template}(x,y))} * 100 \quad , \qquad (16)$$

where P is the percentage of the overlapping area. *m* and *n* are the number of rows and columns of the image respectively. $I_{template}(x,y)$ and $I_{skull}(x,y)$ are the pixel intensity at *(x,y)* position in the template and bone respectively. After the percentage of overlapping area is determined for each template, decision rules presented in Table 1 are employed to identify the location of the CT image.

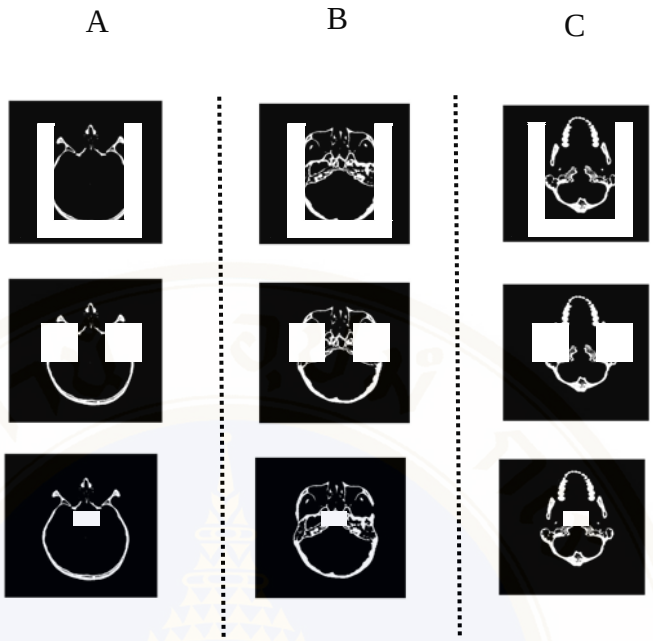

Figure 2.32 Example of comparing different skulls with templates;
A) The skull is above orbital sockets.
B) The skull is between orbital sockets and hard palate.
C) The skull is below hard palate.

Table 1 Decision rules for CT image location identification

	Percentage of the overlapping area		
Decision Rules	**Template I**	**Template II**	**Template III**
Above orbital sockets	High	High	Low
Between orbital sockets and hard palate	High	High	High
Below hard palate	Low	High	Low

2. Image normalization

Because CT Images perhaps gain from different sources and operators, their intensity range may be different [23]. In general, the CT images in Hounsfield units are changed into 12 bit intensity values, i.e. between 0 and 4095. After that, the operators or radiologists may adjust the CT scale to different intensity range for the ease of visualization. For example, it may be scaled in the range of [0 3565] to visualize the skull. Before analysis, each CT image is normalized to the 12 bit intensity values by

$$I(x,y) = \frac{4095}{max-min} * (I_0(x,y) - min) \quad (17)$$

where $I_{(x,y)}$ is the normalized pixel intensity, max and min indicate the maximum and minimum intensity values of the CT image prior to the normalization respectively.

3. Generation of representative images

Due to the fact that NPC regions in CT images may have different locations, patterns, and intensities, representatives of these images are constructed. Self-Organizing Map which is an unsupervised learning technique is exploited to create topological maps which are used as the representative images. Initially, all normalized CT images are separated into two groups, i.e., training and testing groups. The training group is employed to create the representative images. The testing group is used in the performance evaluation. Each m x n normalized image is reshaped into a 1 x (m x n) matrix (row vector). In the similar manner, the representative image is formed by a weight vector of size 1 x (m x n). The number of weight vectors must be specified. These weight vectors are randomly initialized. Their values are adjusted through the competitive learning process. Weight vectors after the learning process from the topological maps. These maps are the representatives of NPC images. Pseudo code of SOM can be presented as follows.

1. Each reshaped image in the training set is used as an input vector

2. For each input, Euclidean distance to all weight vectors is calculated by $d_k = \sqrt{\sum_{i=1}^{m}\sum_{j=1}^{n}(I(i,j) - W_k(i,j))^2}$ *(18)*

3. Select the best matching unit (BMU), which is the most similar to the input vector, and its neighbors. Figure 2.33 shows BMU and its neighbors.

4. Weights of BMU and its neighbors are adjusted according to Eqs. (19) – (22). Neighboring of BMU is an exponential decay function given by Eq. (22).

$$W(t+1) = W(t) + \theta(t)\alpha(t)(I(t) - W(t)) \quad , \quad (19)$$

$$\alpha(t) = \alpha_0 e^{-\frac{t}{\lambda}} \; ; \; t = 1,2,3\ldots \quad , \quad (20)$$

$$\theta(t) = e^{\left[-\frac{d^2}{2\sigma^2(t)}\right]} \; ; \; t = 1,2,3\ldots \quad , \quad (21)$$

$$\sigma(t) = \sigma_0 e^{-\frac{t}{\lambda}} \; ; \; t = 1,2,3\ldots \quad , \quad (22)$$

where σ is the radius of BMU neighborhood, λ represents the time constant, and t denotes the number of iterations. Both σ and α are monotonically decreasing functions. Neighboring radius of BMU is gradually reduced over iterations until neighboring weight vector does not exist.

5. Repeat step 2-4 until no weight change.

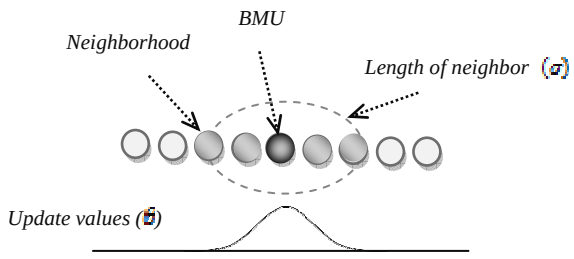

Figure 2.33 BMU and its neighbors

Example of the topological maps during the learning process can be shown in Figure 2.34

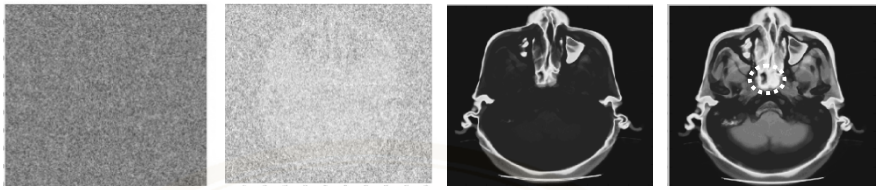

a) Initial b) 1st iteration c) 200th iteration d) 800th iteration

Figure 2.34 Example of represent image generated by SOM technique over iterations.

Figure 2.34d) presents the representative image created at 800th iteration of learning. The dashed circle indicates the tumor area which is obviously different from nearby area. Location of the tumor region in the representative image is used in the segmentation.

4. Mode of NPC determination

After all representative images are generated, the image that is the most similar to a CT of interest is chosen from minimum Euclidean distance measure. User has to specify an initial seed on the CT image. Location of the seed is marked onto the selected representative. At this location, a 9x9 mask is placed. Mode of representative image intensities within this mask is determined and used for region growing segmentation. By doing this, inappropriate seed selection on the CT image can be reduced. Locations of the segmented regions are used for retrieving image intensities on the CT image. Mode of these intensities is determined. Mode intensity and the intensity of the seed point are used in the segmentation. In this thesis, they are used in the region growing technique.

5. Region growing using mode intensity and location of the initial seed point

Region growing technique in this thesis is modified from Adams and Bischof [14]. Tumor pixel (seed) is initially specified. Its neighboring pixels are collected. Difference between the tumor pixel intensity and intensity of each neighboring pixel, $\delta(x)$, is determined. Pixel having minimum difference is selected.

It is included as tumor pixel when its intensity is within the predefined range, ∂. The algorithm searches all nearby pixels until no tumor pixel is added. After the tumor pixel is added, intensity difference, $\delta(x)$, is determined from

$$\delta(x) = |g(x) - mean_{y \in A}\{g(y)\}| \quad , \quad (23)$$

where $g(x)$ represents intensity of pixel x. $mean_{y \in A}\{g(y)\}$ is the average value of tumor pixel intensities. In this thesis, the intensity difference is calculated from

$$\delta(x) = |g(x) - mode\{g(y_{SOM})\}| \quad , \quad (24)$$

where $mode_{y \in A_r}\{g(y_r)\}$ is the mode intensity specified by SOM.

Range of growing, ∂ is computed from adding the mode intensity with certain constant value C as

$$\partial = mode\{g(y_{SOM})\} \pm C \quad , \quad (25)$$

Appropriate constant value is investigated in experiment 1. After the NPC region is segmented, it may contain holes and unsmooth boundary. Post processing is required. In this paper, image morphology techniques are applied. Image dilation and erosion are employed. An example of segmented tumor region after applying the post processing technique can be shown in Figure 2.35.

a) b)

Figure 2.35 Post processing processed image
a.) prior to applying post processing technique
b.) after applying post processing technique

2.6.4 3D Visualization

After tumor region is marked on a CT image, 3D model of the tumor can be visualized. Surface rendering and volume rendering functions are provided. Each function is described as follows.

1. Surface rendering function. For this function, marching cube technique is employed. 3D models of the tumor and patient's skull are constructed and displayed concurrently as presented in Figure 2.36.

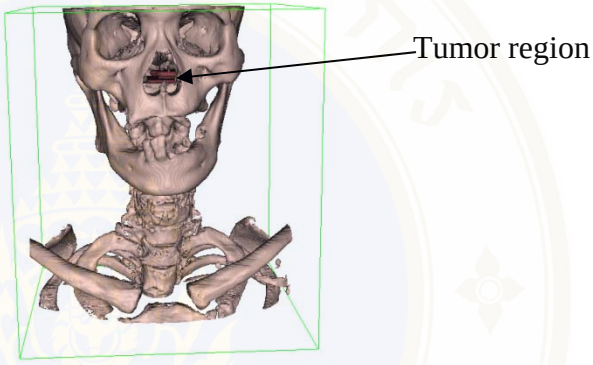

Figure 2.36 3D model from surface rendering function

2. Volume rendering function. For this function, volume ray casting technique is exploited. Example of the 3D model constructed by this function is shown in Figure 2.37.

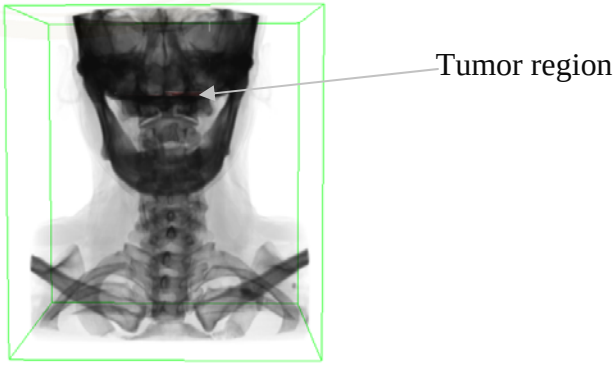

Figure 2.37 3D model from volume rendering function

Finally, volume of the 3D model is calculated by counting the number of voxels in the 3D generated data. For volume rendering method, the volume can be estimated by simply counting voxels inside the reconstructed objects plus a half of total voxels along the surface. In case of surface rendering, Divergence Theorem algorithm (DTA) [24] is employed to determine the tumor volume from surface contour. In this study, VTK [25] is utilized in order to visualize the 3D reconstruction model. vtkMassProperties function is exploited to determine the volume of reconstructed 3D model. The estimated volume is presented in a message box as shown in Figure 2.38.

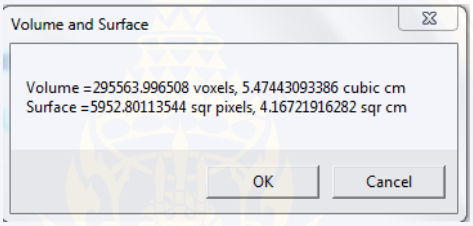

Figure 2.38 Volume and surface estimation of a 3D model (in centimeter)

CHAPTER III
MATERIALS AND METHODS

3.1 Materials

3.1.1 Literature Resource

Journals and papers reviewed in this research were gained from electronic resources access via Mahidol University subscriptions. DICOM files of NPC patients were obtained from faculty of medicine, Ramathibodi hospital, Mahidol university. Standard ground truth images were created from 3 experienced radiologists.

3.1.2 Hardware Resource

The software had been developed under the following computer's specification:

CPU : Intel® core 2 duo E7500 2.93 GHz
RAM : 4 GB
HDD : 500 GB
VGA card : GMA X4500

Minimal requirements to run this software were summarized below:

CPU : Intel® Pentium 4 or equivalent
RAM : 512 MB for segmentation and 1 GB for 3D reconstruction
HDD : at least 1 GB free space
VGA card : 16, 24, or 32 bit OpenGL compatible
Other peripherals:
Monitor, mouse, and keyboard.

3.1.3 Software Resource

Operating system : Windows® seven 64bit ultimate edition
Programming tool : MATLAB® R2008a
3D Rendering tool : VTK

3.2 Methodology

In this session, research methodology is presented. It can be summarized as shown in Figure 3.1.

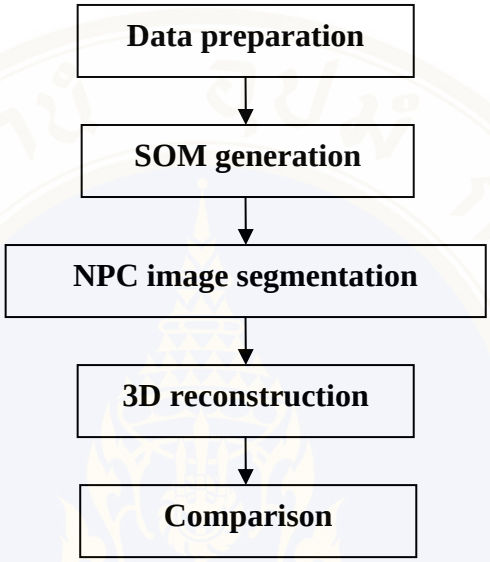

Figure 3.1 Research methodology

3.2.1 Data preparation

CT images of 31 patients with nasopharyngeal carcinoma, who were treated at Ramathibodi hospital, were collected and stored in DICOM file format. This research has been approved by the Ethic Committee of Mahidol University. Standard ground truth images were obtained from 3 experienced radiologists.

3.2.2 SOM generation

In this step, SOM is developed in order to generate representative of NPC images. Because some standard ground truth images contain non-overlapping or partially overlapping tumor regions, in order to create efficient representative images, CT images having the corresponding ratio (CR) less than 0.5 are discarded from SOM generation. The corresponding ratio is determined from their ground truth images. Figure 3.2 shows standard ground truth images having low and high corresponding ratios.

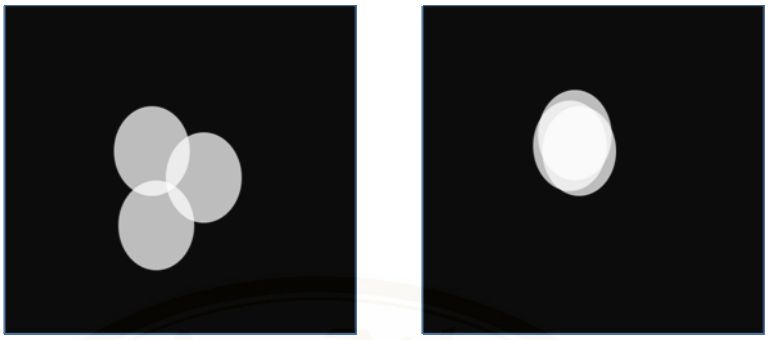

a) CR<0.5 b) CR>0.5

Figure 3.2 standard ground truth images

Experiment 1 Appropriate number of representative images and bound of region growing determination.

This experiment aims to investigate appropriate number of representative images and bound of growing. SOM networks consisted of 10, 20, and 30 representative images are constructed. Constant used for defining region growing is finely tuned from 10 to 20 with the incremental of 0.5. Single seed selected from centroid of overlapping tumor regions is used as initial seed point. Figure 3.3 shows an example of seed selection from 3 overlapping ground truth images. This seed is used in the segmentation. In performance evaluation, common ground truth image is generated and compared with the segmented region. This common ground truth is created from intersection of tumor regions specified by 3 radiologists. By doing so, the selected number of representative images and bound can be ensured to provide accurate NPC region segmentation in each image. Differed judgment of radiologists is avoided.

Appropriate number of representatives and the constant which provide highest CR is used for the segmentation in further study. Because CT images are categorized into 3 groups, their appropriate number of representative images and bound may be different. These parameters are thus separately determined.

Figure 3.3 Seed point selected from centroid of overlapping tumor regions

3.2.3 Image segmentation

In this part, NPC image segmentation using the proposed technique is investigated. The number of representatives and bound constant from experiment 1 are used in the study. CT images having the corresponding ratio (CR) less than 0.5 are included. Two experiments are performed for performance evaluation. In each experiment, each group of CT images is separately tested.

Experiment 2 SOM based segmentation

This experiment aims to evaluate NPC region segmentation performance from the proposed technique when it is used in a real situation. Assume that the developed software is separately used by 3 radiologists. Initial seed is thus selected differently for each one. In the experiment, the seed point is chosen from centroid of each ground truth image. After the segmentation, the segmented region is compared with the corresponding ground truth. For example, if the seed is selected from the ground truth image of radiologist 1 (GT1), CR and PM are measured from the GT1. Because the performance evaluation is individually performed for each radiologist, all excluded images which their CR below 0.5 can be taken into consideration. After the first seed is used in the segmentation, the second seed is created in order to fulfill the segmented region. This seed is selected from the centroid of unsegmented tumor region determined from each ground truth image. Segmented areas from these seeds are integrated. CR and PM of the total area thus are measured and used in performance evaluation.

3.2.4 Comparison

This part studies NPC image segmentation using traditional region growing based technique. Appropriate bound of growing is determined and used in the segmentation. The segmented region is then compared with that of the proposed technique. Each group of CT images is separately tested.

Experiment 3 Appropriate bound of region growing determination.

This experiment aims to determine appropriate bound of traditional region growing technique. Seed selection and performance evaluation are performed in the

similar manner of experiment 1. Bound of region growing is varied from 10 to 50. CR for each bound is measured by comparing the segmented region with the common ground truth image. The bound which provides the best segmentation is selected and used in further study.

Experiment 4 Performance Comparison

In this experiment, segmentation performances from traditional region growing technique are measured. Appropriate bound from experiment 3 is employed in the experiment. Seed selection and performance evaluation are performed in the similar manner of experiment 2. Segmented region is compared that of the proposed technique.

3.2.5 3D reconstruction

In this part, two experiments about 3D reconstruction are performed. They are volume estimation of 3D models and 3D visualization of tumor model displayed in the skull.

Experiment 5 Volume determination of geometry models

3D virtual models including cubic, cylinder, and ellipsoid are generated. These models are sliced into multiple 2D images and reconstructed into 3D models through the volume rendering technique. Each model consists of 200 2D images. Figures 3.4-3.6 present examples of 2D images from each model. Volume of the model is computed from the number of voxels and compared with its geometry. Correlation percentage is employed in the comparison. It is determined from dividing the estimated volume by the geometrical volume. The result is multiplied by 100. If the percentage is 100%, the estimated volume is equal to the geometrical volume.

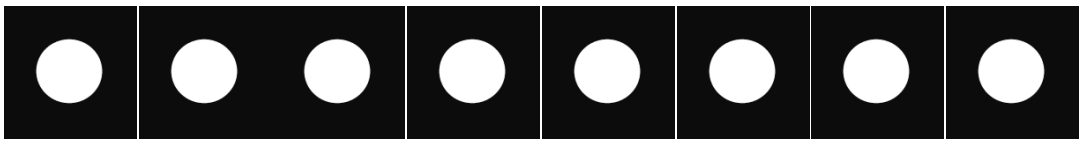

Figure 3.4 2D images of cylinder model

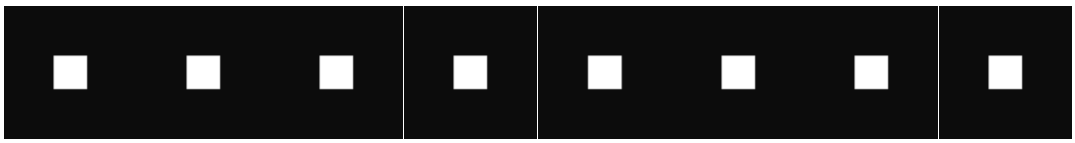

Figure 3.5 2D images of cubic model

Figure 3.6 2D images of ellipsoid model

Experiment 6 3D visualization of tumor model displayed in the skull

After NPC image segmentation is performed, 3D tumor model is generated from the segmented regions. The reconstructed tumor model is displayed in the skull for both surface and volume rendering techniques. Surface of the tumor model is presented by red color.

CHAPTER IV
RESULTS

4.1 Data preparation

The proposed segmentation techniques were applied to CT images of patients with nasopharyngeal carcinoma who were treated at Ramathibodi hospital, Thailand. 6,606 CT images from 31 patients were collected from NPC patients who admitted at Ramathibodi hospital since 1982-2007. The cancer stages cover stage I to Stage IV. Only 578 images contain tumor as specified by 3 experienced radiologists. An example of NPC image and its ground truth images can be shown in Figure 4.1. All collected CT images can be summarized as presented in Table 4.1.

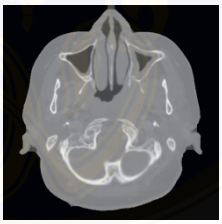

a) An example of CT image

b) GT1 **c) GT2** **d)GT3**

Figure 4.1 NPC image and its standard ground truth images

a) Original NPC image
b) Ground truth from radiologist 1
c) Ground truth from radiologist 2
d) Ground truth from radiologist 3

Table 4.1 All CT images

Patient	Tumor Stage	Number of CT images	Number of tumor images	Groups		
				I	II	III
1	T4	282	35	6	19	10
2	T1	261	8	-	8	-
3	T3	261	7	-	7	-
4	N/A	237	3	-	3	-
5	T1	281	16	-	-	16
6	T3	282	10	-	10	-
7	T3	282	20	-	9	11
8	T2	282	25	-	13	12
9	T4	281	49	-	-	49
10	T2	231	10	-	10	-
11	T4	231	8	-	8	-
12	T2	281	12	-	-	12
13	T4	236	47	-	16	31
14	T4	282	31	-	19	12
15	T4	281	13	-	13	-
16	T4	222	1	-	-	1
17	T4	282	4	-	4	-
18	T4	281	48	-	19	29
19	T4	264	28	-	23	5
20	T4	199	29	-	21	8
21	T4	229	25	-	25	-
22	T4	202	16	-	16	-
23	T4	238	12	-	12	-
24	T2	275	15	-	14	1
25	T3	272	12	-	12	-
26	T3	265	20	-	20	-
27	T3	235	14	-	12	2
28	T2	199	15	-	15	-
29	T1	214	23	-	14	9
30	T2	432	11	-	11	-
31	T2	216	11	-	11	-
	Total	**6606**	**578**	**6**	**364**	**208**

4.2 Image Segmentation

After the CT images were collected, two image segmentation techniques presented in chapter II were applied. They were seeded region growing based on SOM network and traditional seeded region growing algorithm. The CT images were classified into 3 groups according to their location. Prior to the segmentation, CT images having the corresponding ratio (CR) less than 0.5 are discarded from experiments 1 and 3. Table 4.2 shows the number of images that was taken into consideration.

Table 4.2 The number of images that was taken into account

Patient	Total Images	No. of Images CR>=0.5	Group of CR>=0.5		
			I	II	III
1	35	0	0	0	0
2	8	0	0	0	0
3	7	0	0	0	0
4	3	0	0	0	0
5	16	1	0	0	1
6	10	0	0	0	0
7	20	5	0	3	2
8	25	13	0	11	2
9	49	30	0	0	30
10	10	0	0	0	0
11	8	0	0	0	0
12	12	0	0	0	0
13	47	29	0	7	22
14	31	21	0	12	9
15	13	1	0	1	0
16	1	0	0	0	0
17	4	1	0	1	0
18	48	19	0	7	12
19	28	7	0	7	0
20	29	14	0	13	1
21	25	22	0	22	0
22	16	16	0	16	0
23	12	12	0	12	0
24	15	15	0	7	8
25	12	11	0	11	0
26	20	15	0	15	0
27	14	0	0	0	0
28	15	9	0	9	0
29	23	0	0	0	0
30	11	3	0	3	0
31	11	1	0	1	0
Total	**578**	**245**	**0**	**158**	**87**

As seen in Tables 4.1-4.2, there existed only 6 images in group I and these images had CR less than 0.5. In this thesis, the segmentation experiments focus only on groups II and III.

Experiment 1 Appropriate number of representative images and bound of region growing determination.

This experiment aims to determine the appropriate parameters for SOM based segmentation technique. The seed determination and performance measurement are evaluated based on common tumor region. Figures 4.2 and 4.3 present corresponding ratio (CR) when varying bound constants for groups II and III respectively. The constants which give the best CR results will be selected.

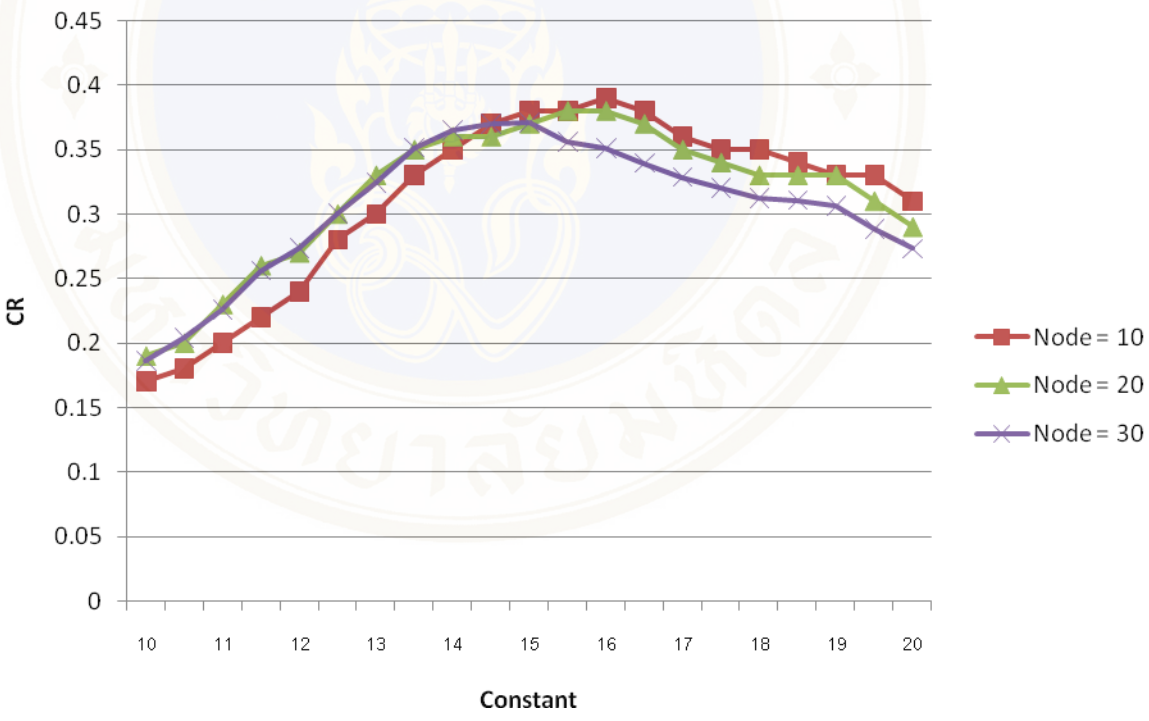

Figure 4.2 CR for each SOM network (group II)

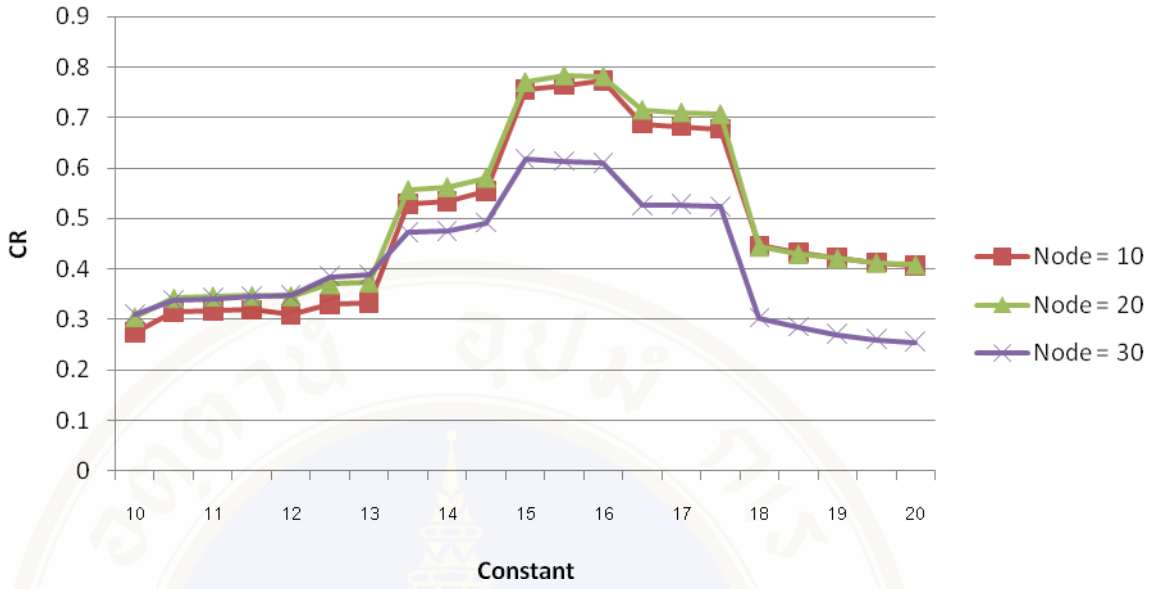

Figure 4.3 CR for each SOM network (group III)

From Figures 4.2 and 4.3, appropriate bound constants for each SOM network are summarized in Table 4.3

Table 4.3 Appropriate bound constant for each group.

	Group II		Group III	
Node	**CR**	**Constant**	**CR**	**Constant**
10	0.39	16	0.78	16
20	0.38	16	0.78	15.5
30	0.37	15	0.61	15

Form Tables 4.3, ten representative images and bound constant of 16 were selected for further experiments because these parameters provided the highest CR. In addition, the number of representative images was low leading to less computational time.

Experiment 2 SOM based segmentation.

This experiment aims to measure the performance of SOM based segmentation. In the experiment, initial seed point was determined from centroid of each ground truth image. The segmented region was separately compared with each ground truth. CR and PM were measured and presented in Figures 4.4 and 4.5.

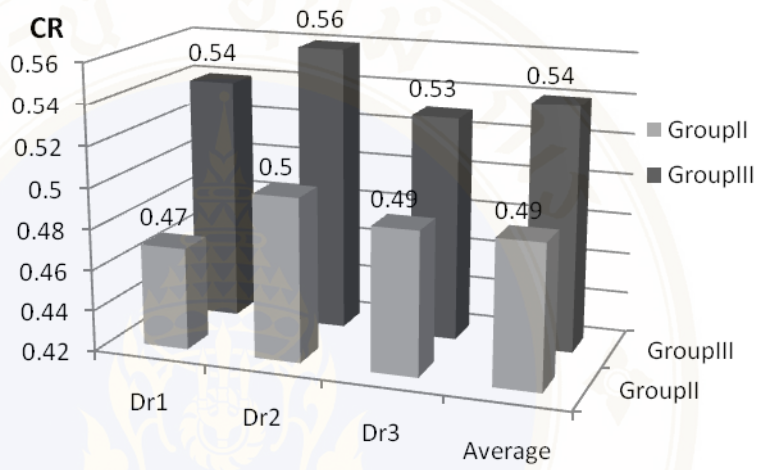

Figure 4.4 CR for single seed SOM based segmentation

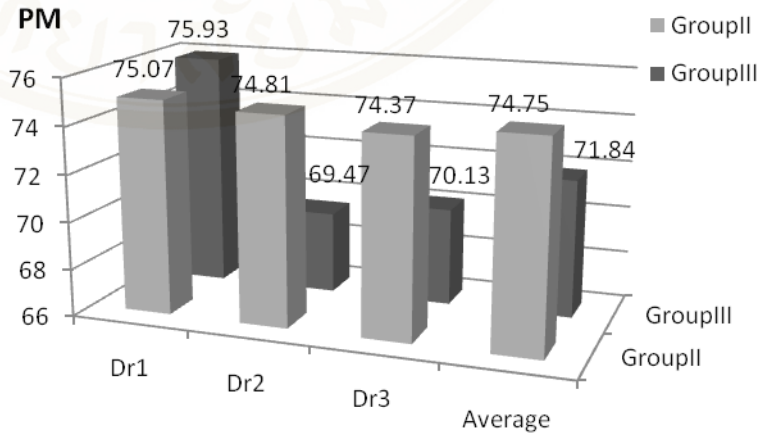

Figure 4.5 PM for single seed SOM based segmentation

From Figures 4.4 - 4.5, average CR for groups II and III were 0.49 and 0.54 respectively. Average PMs were 74.75 and 71.84 for groups II and III. The segmented

regions were slightly different from that of each radiologist. Unsegmented region were continually considered. Figures 4.6 and 4.7 present two seed segmentation performances.

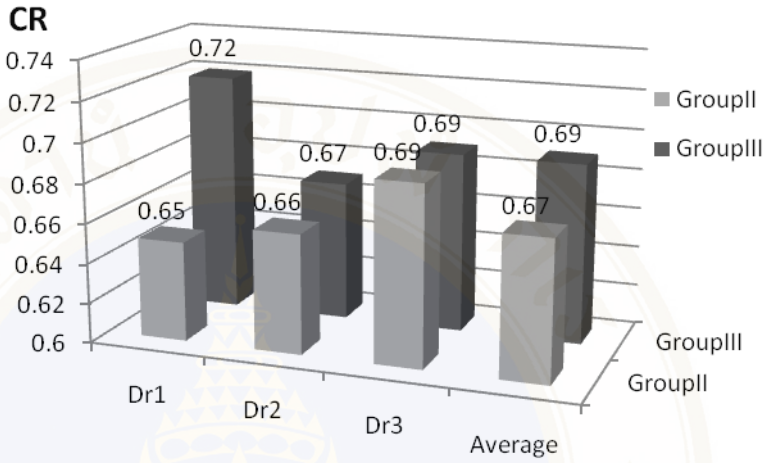

Figure 4.6 CR for two seed SOM based segmentation

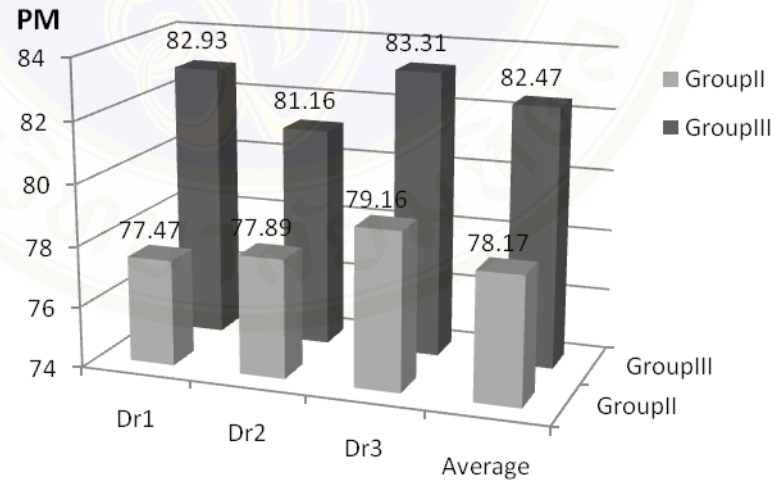

Figure 4.7 PM for two seed SOM based segmentation

From the experimental results, average CRs were 0.67 and 0.69 for groups II and III respectively. Average PMs were 78.17 and 82.47. Higher CR and PM can be gained with the increasing number of seeds.

From the experimental results, CR for group III was higher than that of group II for both single and two seed segmentation. Segmentation performances from this

experiment were compared with that of the traditional region growing approach as presented in experiment 4.

4.3 Comparison

Experiment 3 Appropriate bound of region growing determination.

Appropriate bound constant for traditional seed growing technique is investigated in this experiment. Initial seed points and performance measurement evaluation were similar to experiment 1. CR for groups II and III are presented in Figures 4.8 - 4.9.

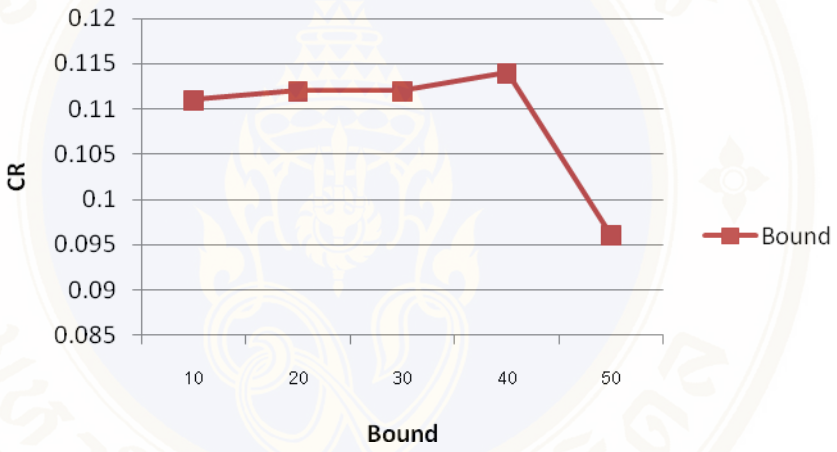

Figure 4.8 CRs after varying bound for traditional seed growing technique (group II)

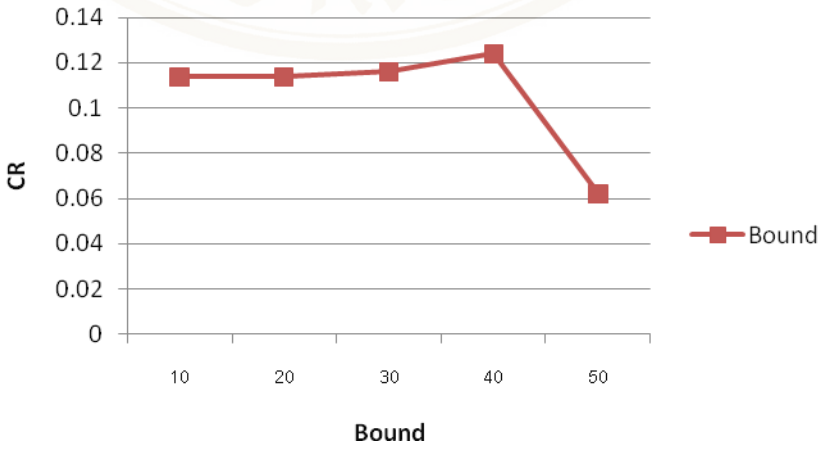

Figure 4.9 CRs after varying bound for traditional seed growing technique (group III)

From Figures 4.8 - 4.9, the bound of 40 provided the highest CR for both groups II and III. It was used in further experiments.

Experiment 4 Performance Comparison

In this experiment, segmentation performances of traditional region growing are investigated and compared with that of SOM based technique. Seed selection and performance evaluation were similar to experiment 2. , CR and PM from single seed segmentation are presented in Figures 4.10 and 4.11.

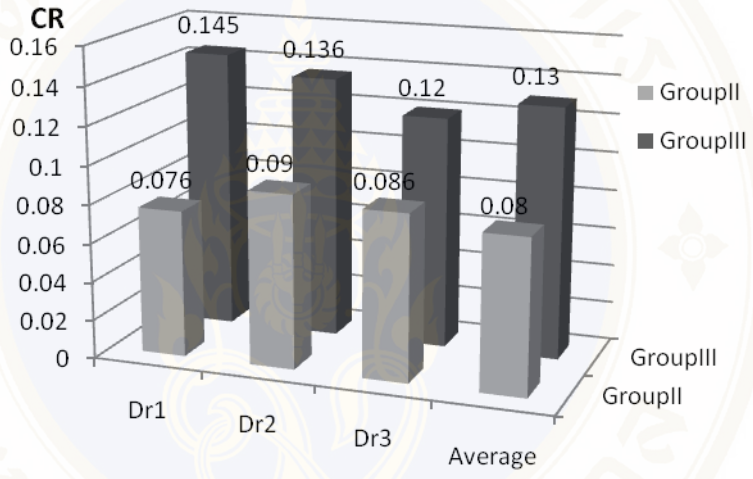

Figure 4.10 CR for single seed region growing

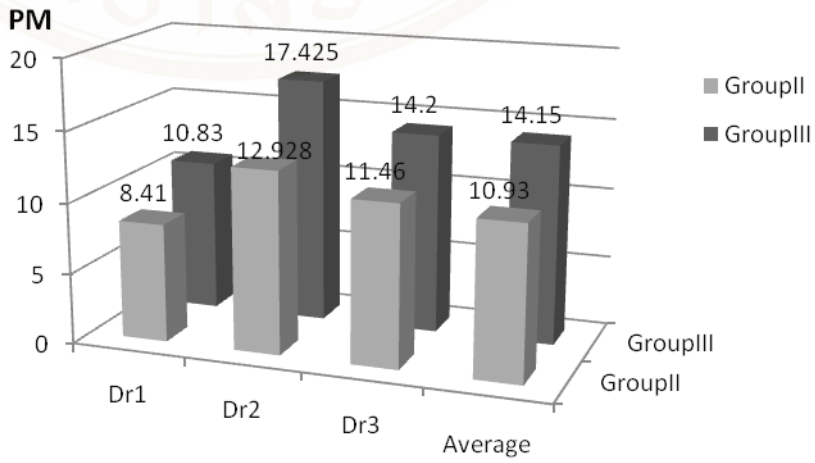

Figure 4.11 PM for single seed region growing

Figures 4.10 and 4.11 show segmentation performances for single seed segmentation. Average CRs for groups II and III were 0.08 and 0.13 respectively. Average PMs were 10.93 and 14.5. In the similar manner, CR and PM for group III were higher than that of group II. Figures 4.12 and 4.13 show CR and PM from two seed segmentation.

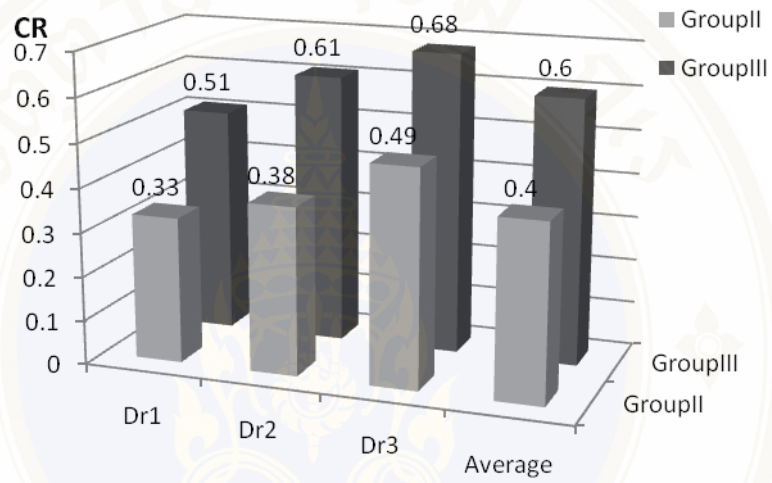

Figure 4.12 CR for two seed region growing

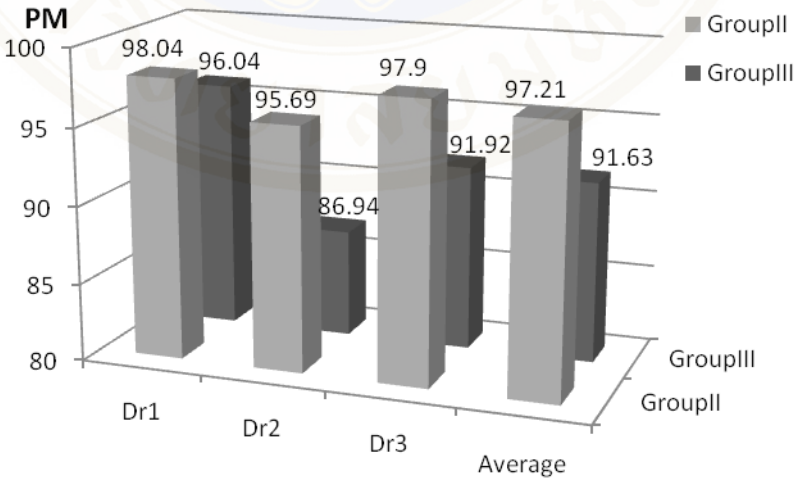

Figure 4.13 PM for two seed region growing

From Figures 4.12 and 4.13, average CRs for groups II and III were 0.4 and 0.6. For PMs, they were 97.21 and 91.63. Higher performances could be achieved with increasing of seeds. Comparison results between SOM and traditional seeded region growing method are presented in Figures 4.14 - 4.17.

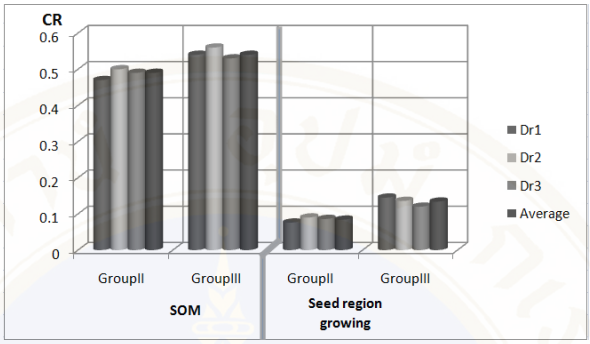

Figure 4.14 Comparison of CR for single seed segmentation.

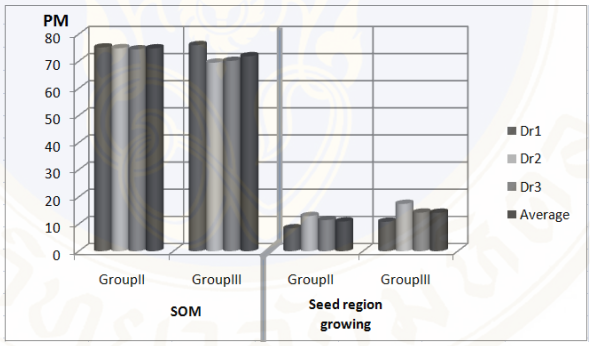

Figure 4.15 Comparison of PM for single seed segmentation

From Figures 4.14 and 4.15, the proposed method provided higher CRs and PMs for both groups II and III. Comparisions for two seed segmentation can be shown in Figures 4.16 and 4.17.

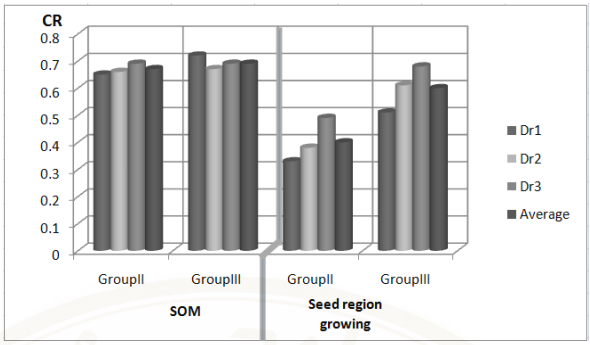

Figure 4.16 Comparison of CR for two seed segmentation

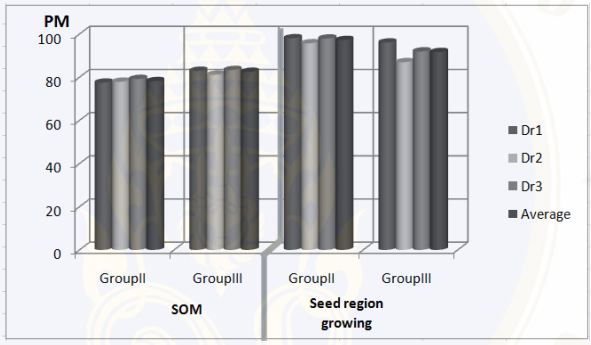

Figure 4.17 Comparison of PM for two seed segmentation

Figures 4.16 and 4.17 show the comparision of two seed performance. For CR, SOM based segmentation was superior to the traditional approach. However, for PM, the traditional method was better. Examples of segmented tumor region from both SOM and traditional region growing based segmentations can be shown in Figures 4.18 – 4.21.

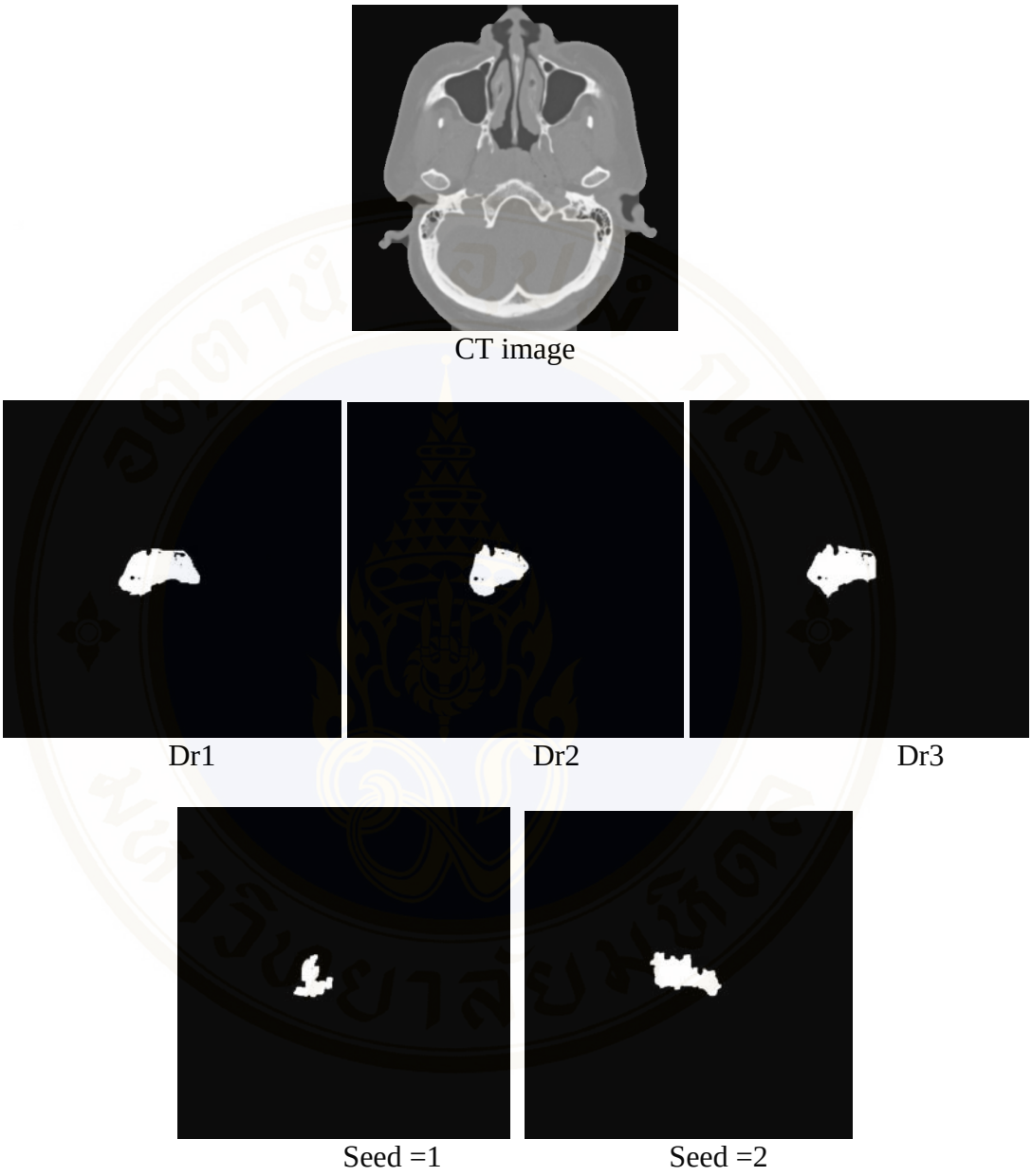

Figure 4.18 Example of SOM segmentation for group II.

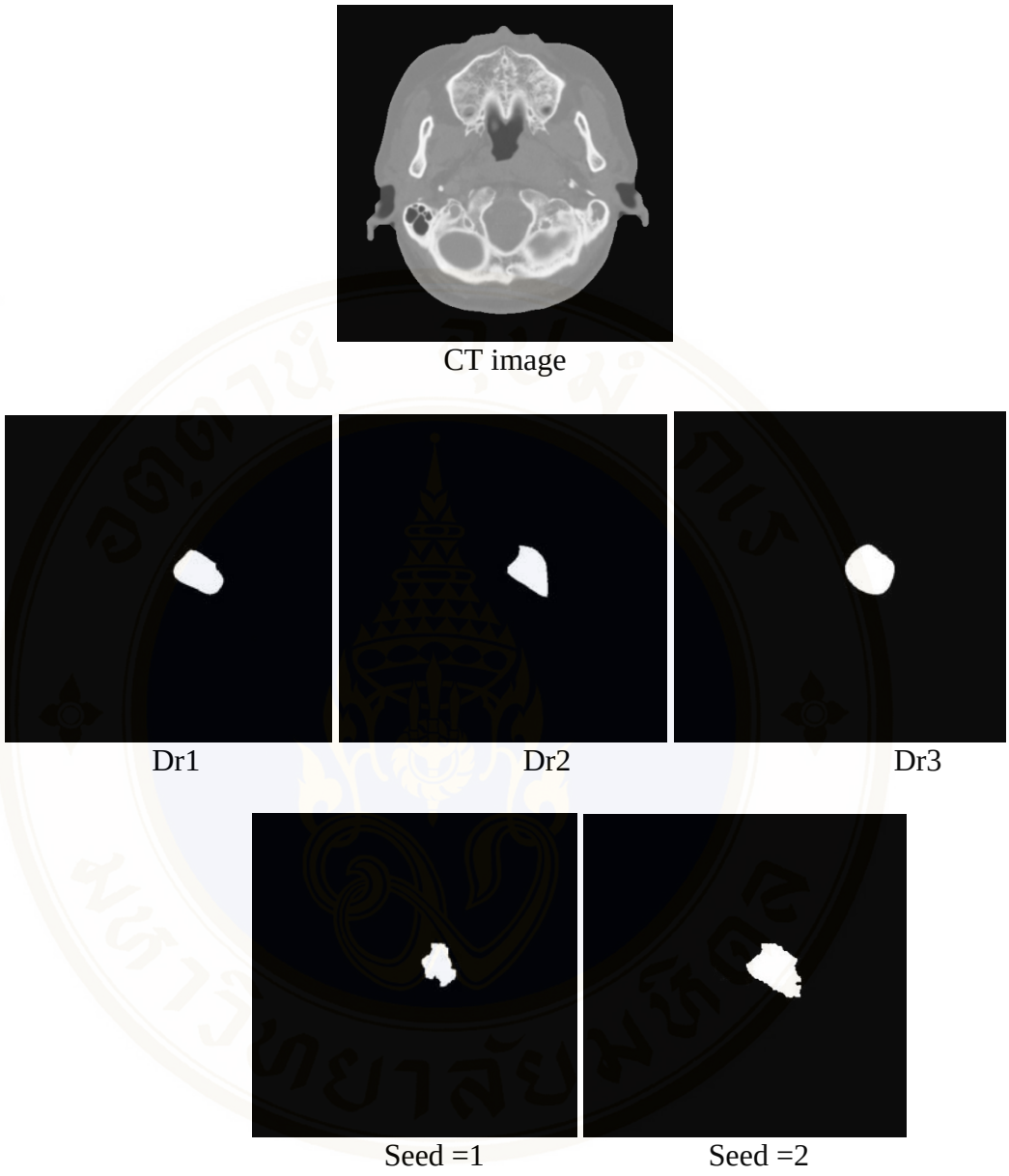

Figure 4.19 Example of SOM segmentation for group III.

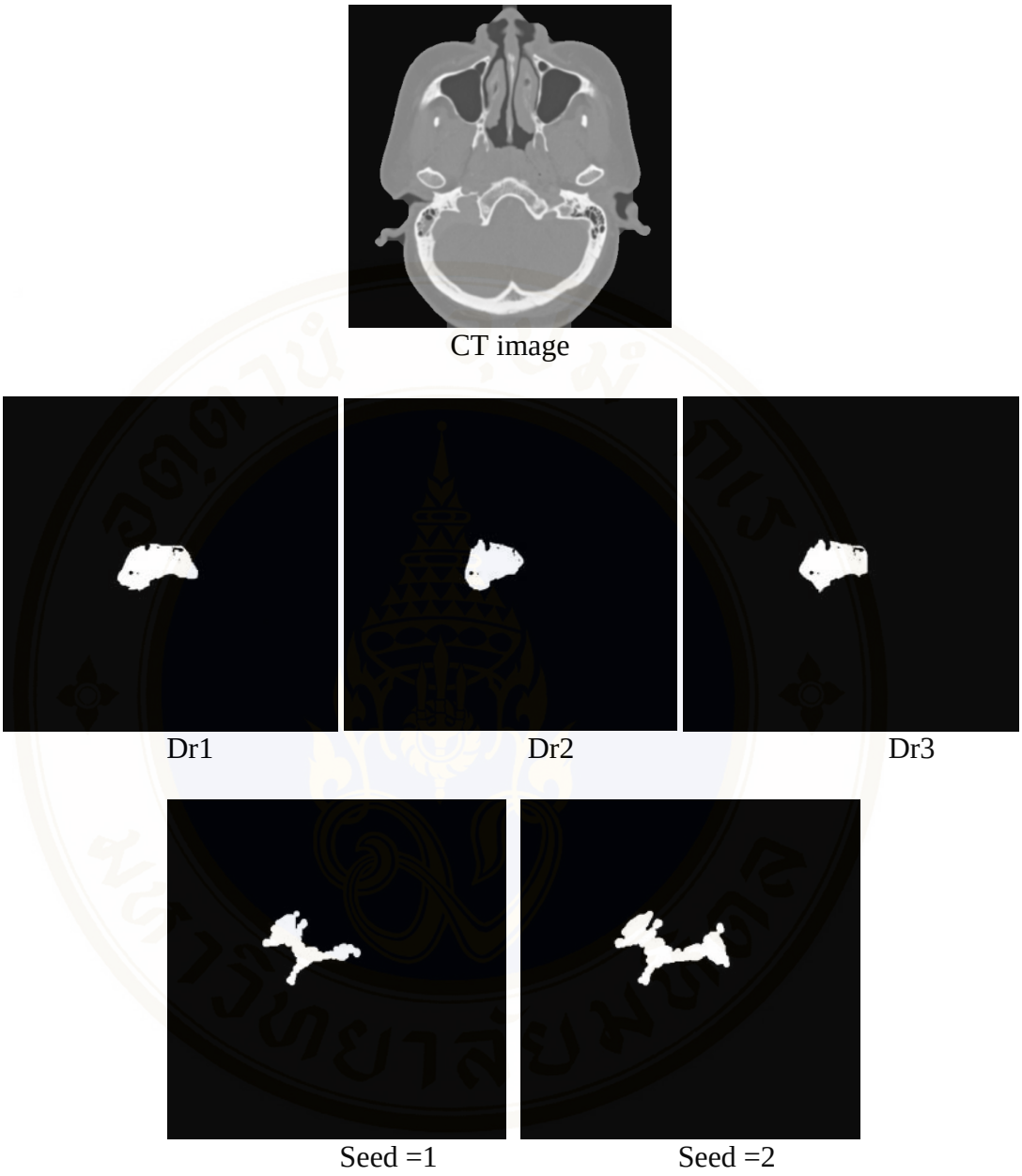

Figure 4.20 Example of traditional seeded region growing for group II.

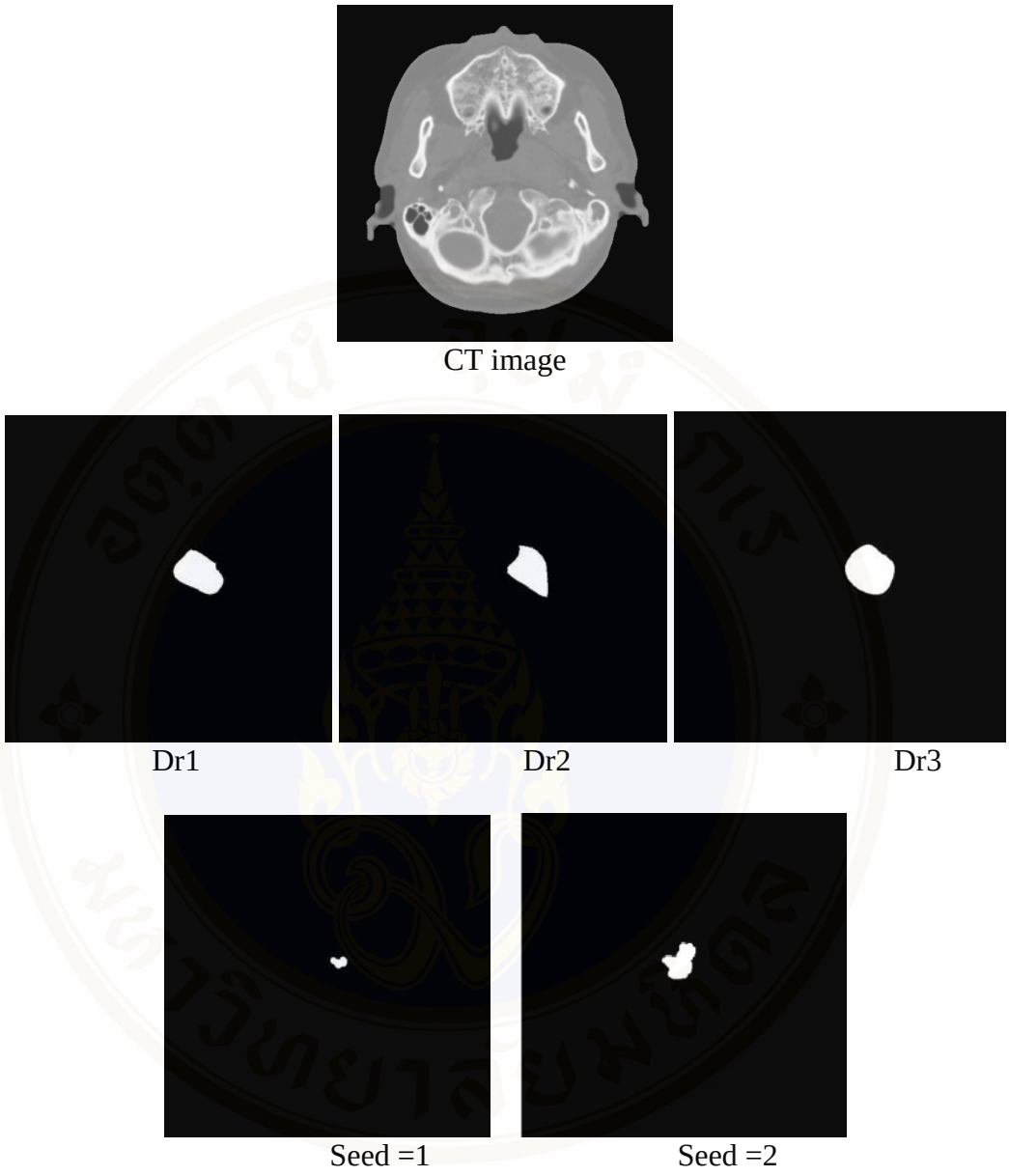

Figure 4.21 Example of traditional seeded region growing III.

4.4 3D Reconstructions

Experiment 5 Volume determination of geometry models.

In this experiment, 2D slices of 3 virtual models are reconstructed. Volume of these models is determined and compared with its actual volume determined from known geometry. Figures 4.22 - 4.24 present the reconstructed models. Volume comparisons are summarized in Table 4.4.

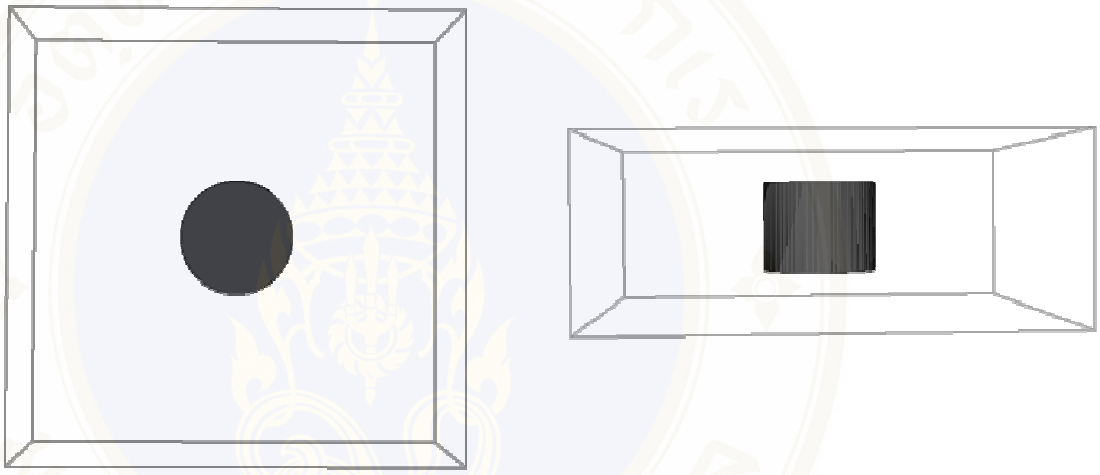

a) 3D cylinder model (Top view) b) 3D cylinder model (side view)

Figure 4.22 Reconstructed cylinder model

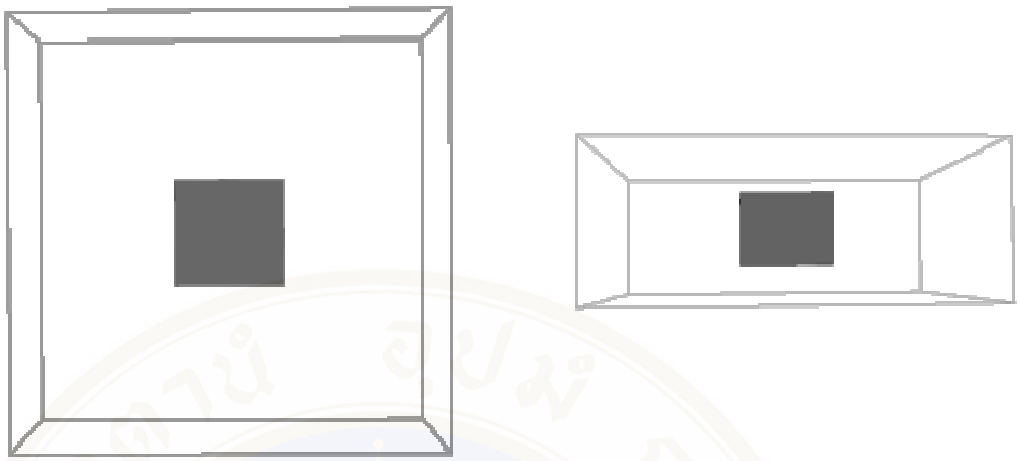

a) 3D cubic model (Top view) b) 3D cubic model (side view)

Figure 4.23 Reconstructed cubic model

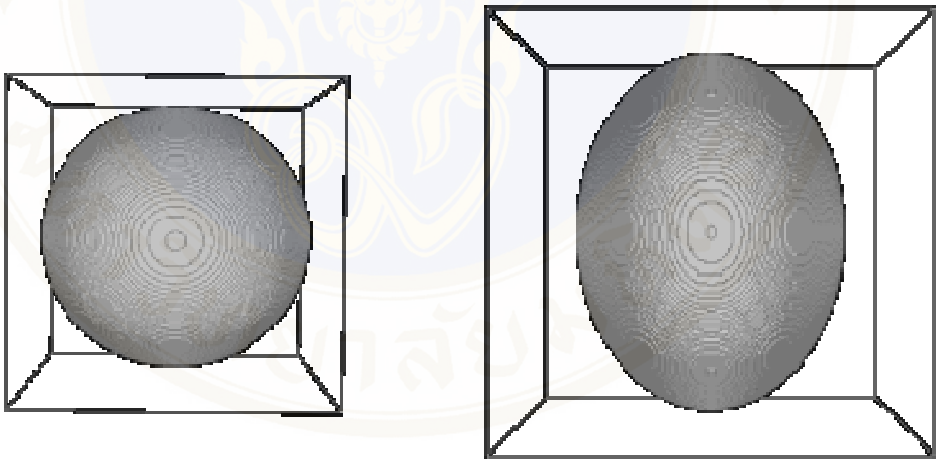

a) 3D ellipsoid model (top view) b) 3D ellipsoid model (side view)

Figure 4.24 Reconstructed ellipsoid model

Table 4.4 Volume Comparisons

Model	Geometrical volume	Estimated volume	Correlation percentage
Cylinder	1286144.000	1352678.264	105.180
Cubic	1638400.000	1656544.058	101.100
ellipsoid	2393139.620	2393234.440	100.003

As seen in Table 4.4, the correlation percentages were 105.18, 101.10, and 100.003 for cylinder, cubic, and ellipsoid respectively. The reconstructed models were thus slightly larger than the actual models.

Experiment 6 3D visualization of tumor model displayed in the skull.

The reconstructed tumor from surface rendering and volume rendering are shown in Figures 4.24 - 4.25.

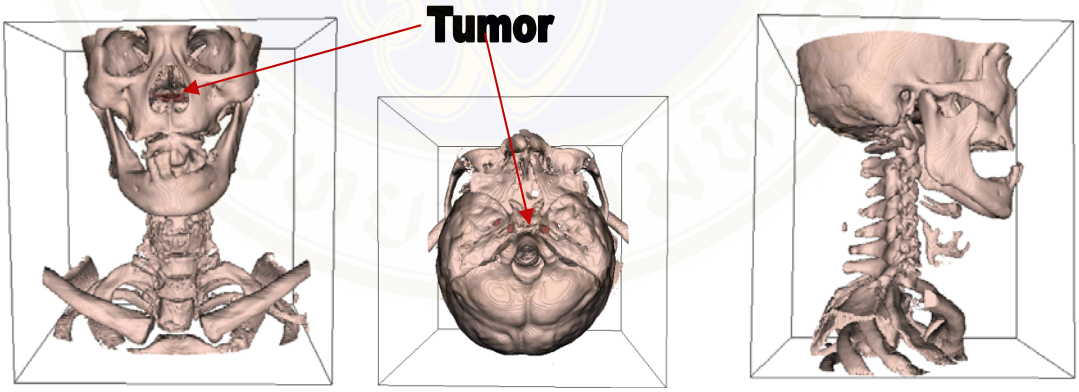

Front view Top View Side View

Figure 4.24 tumor model from surface rendering.

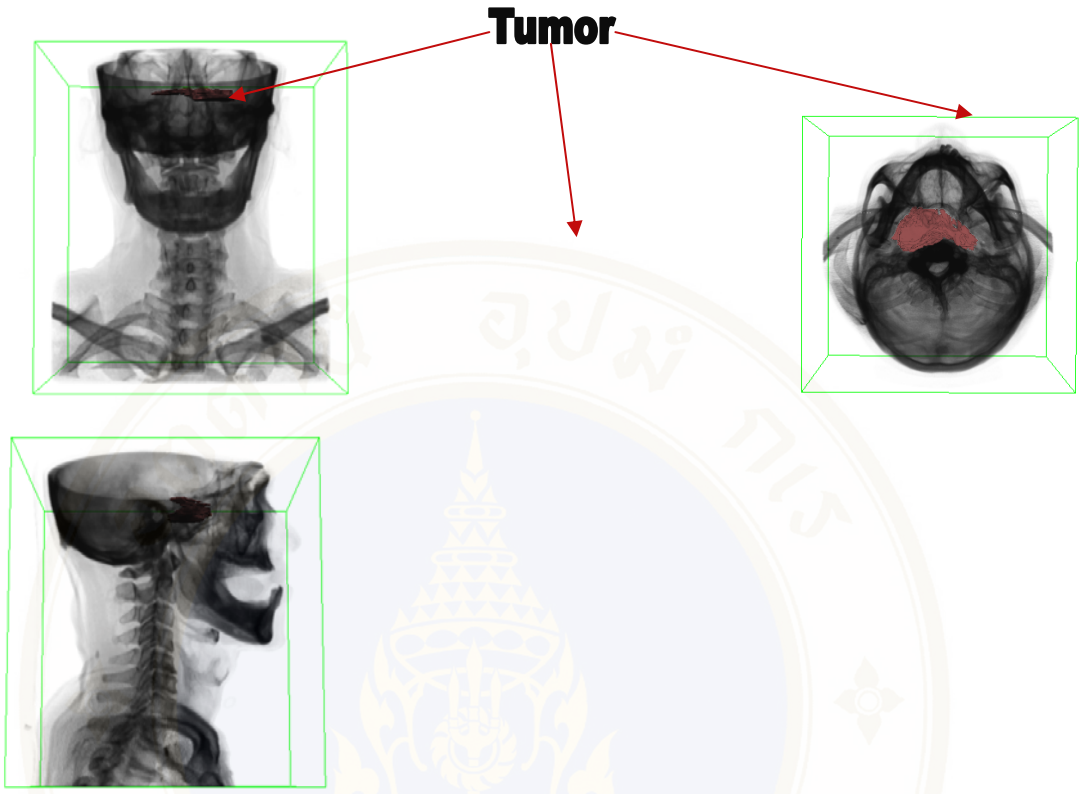

Figure 4.25 tumor model from volume rendering

CHAPTER V
DISCUSSION

In this thesis, there are two main studies, i.e., nasopharyngeal carcinoma (NPC) image segmentation and construction of 3D tumor model. For the image segmentation part, CT images which the corresponding ratio less than 0.5 were excluded from SOM network generation. Uncorrelated ground truth images occurred from unclear border of NPC tumor. Intensities of tumor border were similar to nearby normal tissues. When the images presented on the screen, it is thus difficult to accurately delineate the tumor region. Figure 5.1 shows an example of uncorrelated tumor contours specified by 3 radiologists.

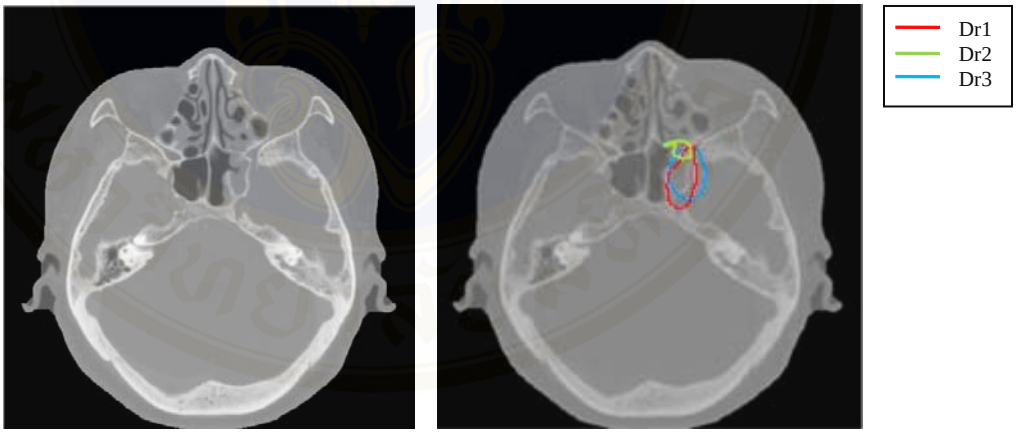

Figure 5.1 Uncorrelated tumor contours

From experiment 1, after varying number of representative images and bound constants, CRs were slightly different. Therefore, the parameters that provided highest CR were chosen. From the results, 10 representative images and bound constant of 16 were appropriate for SOM generation. Small number of representative images could reduce computational time.

Experiment 2 investigated SOM segmentation performance. Segmented regions were compared with ground truth images from each radiologist. Average CRs of three radiologists were 0.49 and 0.54 for group II and group III respectively. This means that a half of tumor region specified by radiologists could be determined by the proposed algorithm. Adding a seed could improve the segmentation performance. CRs for two seed segmentation were 0.67 and 0.69 for groups II and III. This is because the unsegmented region is subsequently segmented from the second seed. Average CR of group III was relatively higher than that of group II. This is probably because the number of images was smaller. Tumor patterns of group III thus have less variation.

For experiment 3, appropriate bound of traditional seeded region growing technique was investigated. Seed determination and performance evaluation were similarly to experiment 1. The bound of 40 was appropriate for both groups II and III, because it provided highest CRs than the other bounds. This bound is relatively higher than the bound of SOM based method. This is due to the SOM based method used the mode intensity from best matching representative image instead of intensity of the seed. The mode intensity represents the intensity that frequently presents in the possible area of tumor. It thus can better represent the tumor pixel than the initial seed which may be differently selected by radiologists. Therefore, the bound constant of growing can be smaller than that of the traditional approach. This bound was used in the experiment 4.

Experiment 4 compared segmentation performances of SOM and traditional seeded region growing approach. SOM was superior to the traditional approach in terms of CRs for both groups II and III. However, PMs of the traditional seeded region growing were slightly higher than that of SOM. This indicated that over-segmentation arose. The segmented region extended to the outside of the ground truth area. Many false positives (*FPs*) occurred leading to low CR. For PM, it considered only true positive (*TPs)*. Figure 5.2 shows an example of segmented area that has many false positives.

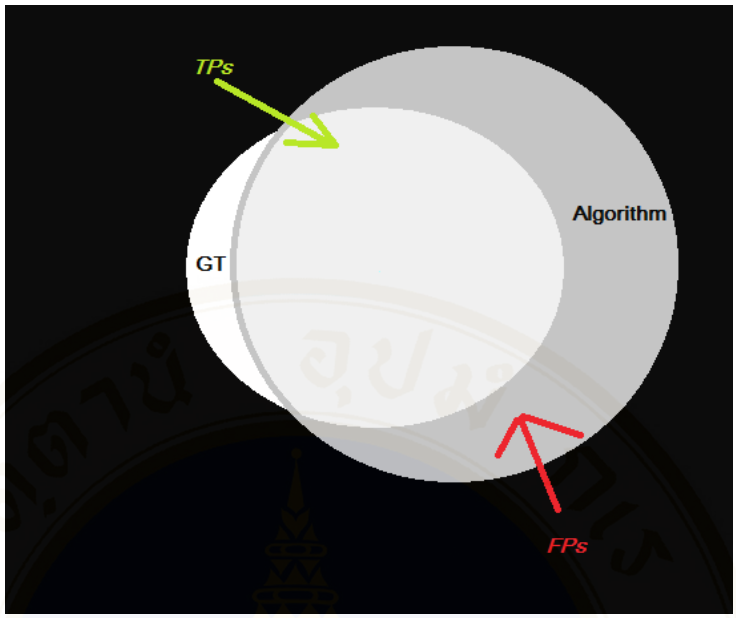

Figure 5.2 Over-segmentation (Low CR, High PM)

Intensity of initial seed plays an important role in the traditional seeded region growing approach especially when an image of interest contains wide range of intensities. Difference of initial seed intensities can generate dissimilar segmented region as shown in Figure 5.3. In this figure, rectangular area represents desired area of segmentation. Initial seed is presented by the black pixel. In Figure 5.3a, the seed has intensity of 11. For Figure 5.3b, the seed is initialized at the upper right corner pixel. Assume that the bound of growing is 10. These two seeds provide different segmented regions. Therefore, intensity of seed is important to the segmentation. SOM based approach uses the mode intensity for growing. It is thus more reliable than using the actual intensity of initial seed that may be different in each identification.

10	11	19	13	15	13	27	30
12	22	10	15	17	15	28	26
11	21	12	22	21	10	12	11
11	14	18	19	19	18	18	12
14	12	20	17	15	15	19	11
10	10	12	10	16	17	14	14

a)

10	11	19	13	15	13	27	30
12	22	10	15	17	15	28	26
11	21	12	22	21	10	12	11
11	14	18	19	19	18	18	12
14	12	20	17	15	15	19	11
10	10	12	10	16	17	14	14

b)

Pixel outsides region bound.

Pixel insides region bound.

Seed point.

Figure 5.3 Seeded region growing when different seed points are initialized

a.) Intensity of initial seed is 11

b.) Intensity of initial seed is 30

From the segmented tumor regions, common site and growth pattern of NPC can be investigated. Figures 5.4-5.7 present integration of tumor region from the ground truth images for each cancer stage. Brightest area indicates tumor region that most frequently found in each group.

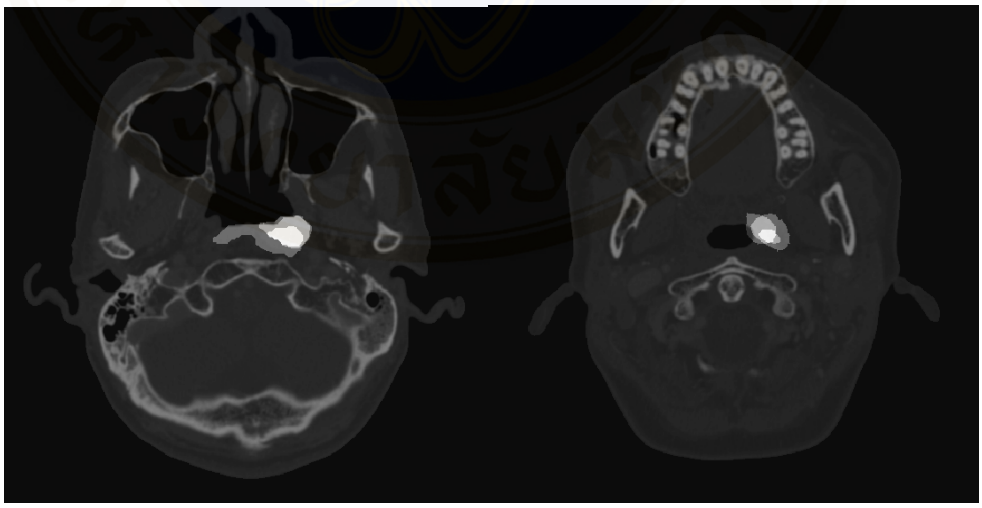

Group II Group III

Figures 5.4 NPC common site of stage I

From Figure 5.4, Tumor is confined within the nasopharynx area, no node involvement and malignant tumor can be observed. From the observations, invasion of

NPC in the stage I usually arise in the right side of the image or the patient's left hand side.

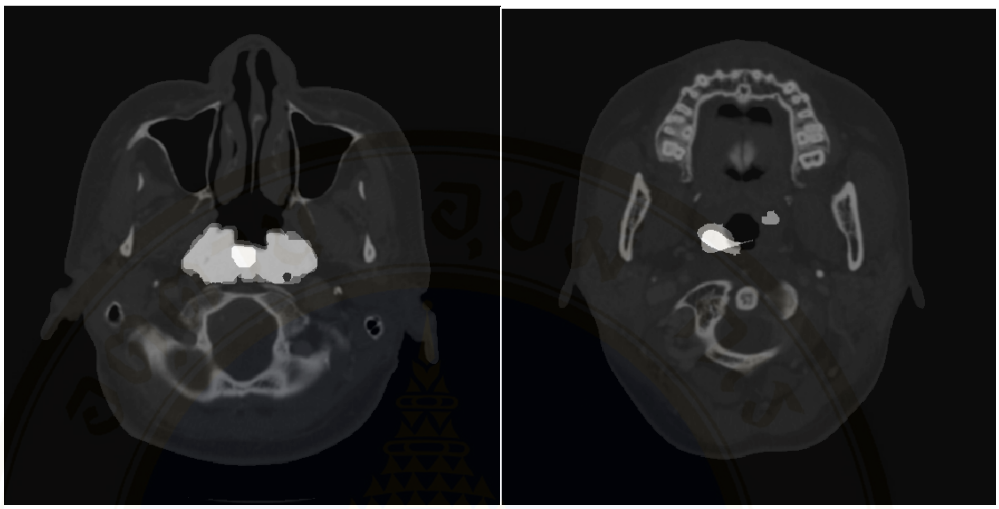

Group II Group III

Figures 5.5 NPC common site of stage II

From Figure 5.5, NPC region for stage II, the tumor involves both sides of nasopharynx and spreads to the border of orropharynx. NPC also invades to the prevertebral muscles, levator palatini muscle and pharyngobasilar fascia. It may involve to the parapharyngeal fat spaces which contains the pharyngeal venous plexus.

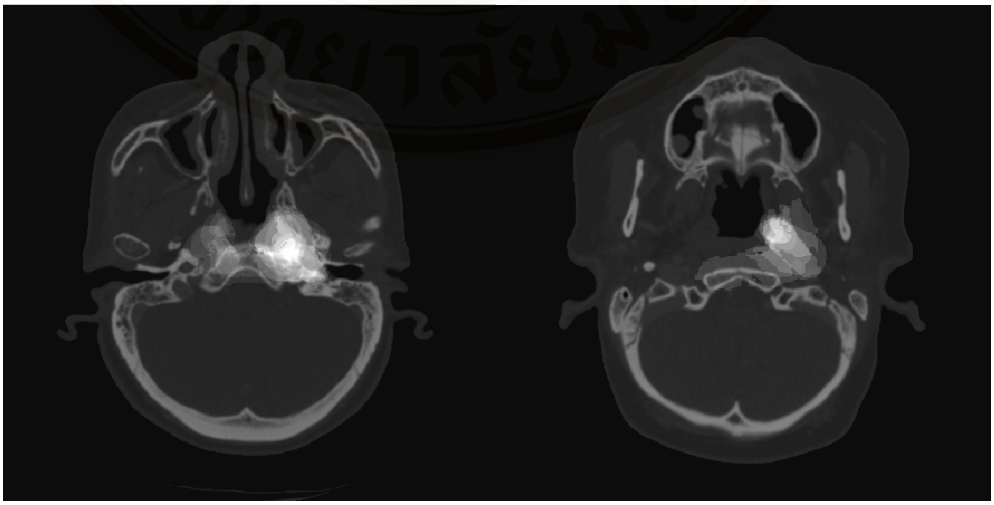

Group II Group III

Figures 5.6 NPC common site of stage III

From Figure 5.6, skull base involvement can be observed. For group II, it is observed considerably that the tumor invades to both left and right sides of the clivus and petrous bones. For group III, it is still commonly found in the right side of image, or the patient's left hand side. The tumor size of group III in this stage is smaller than that of the stage II. This may be because tumor in the stage III usually confines in the upper part of the skull. Thus, tumor is this stage usually occurs in group II. From the literature survey, clivus, pterygoid bones, body of the sphenoid and apices of the petrous temporal bones are mainly invaded areas. However, the tumor may occasionally invade to Sphenoid wings, upper cervical spine, hypoglossal nerve canal, and jugular foramen.

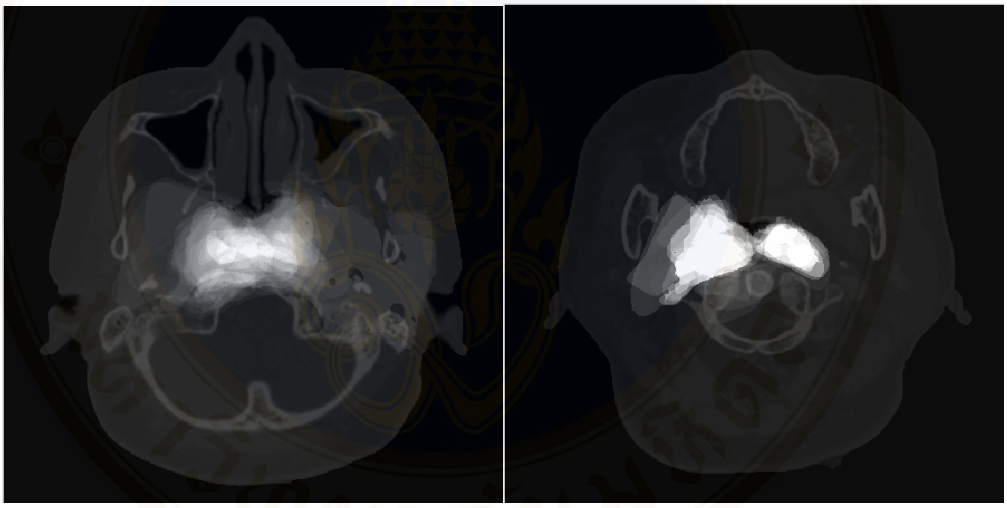

Group II Group III

Figures 5.7 NPC common site of stage IV

From Figure 5.7, the tumor size is obviously large. The tumor involves both sides of nasopharynx and invades oropharynx, central skull base as divus petrous bones, prevertebral muscles, and sphenoid bone. NPC in this stage usually invades to cavernous sinus, horizontal portion of the internal carotid artery, cranial nerves, infratemporal fossa, hypopharynx, orbital fissures, or through the skull base in the region of the foramen ovale or sphenoid sinus.

For 3D reconstruction part, two rendering techniques are investigated, i.e. surface rendering and volume rendering approaches. The surface rendering creates the iso-surface in 3D reconstruction while volume rendering generates voxels from 2D

slices. Volume estimated from the reconstructed models is slightly larger than the actual volume. This error is due to the quantization effect. The virtual model is sliced into 2D images. Then the contour of model is discretized and stored in the array of pixels. Curvature of the contour may shrink or expand as presented in Figure 5.8. This effect causes the surface of 3D reconstructed models was different from the actual.

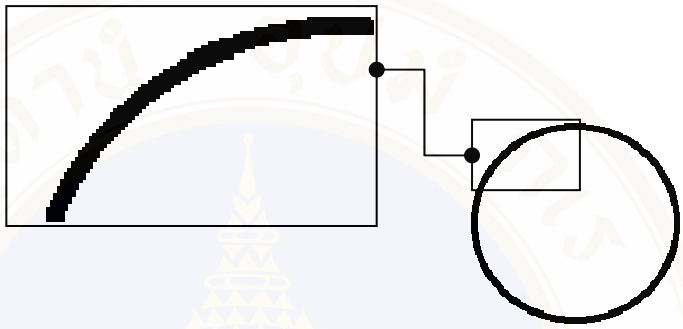

Figure 5.8 Quantization effect

In experiment 6, the reconstructed tumor model was presented. This showed that 3D visualization was successfully developed. The 3D reconstructed model is useful for observing common site and growth pattern of NPC.

CHAPTER VI
CONCLUSION

This thesis studies semi-automatic image segmentation and 3D visualization of nasopharyngeal carcinoma from CT images. There are two major parts. The first part investigates the segmentation of NPC by the use of self organizing map (SOM) based approach. CT images of patients with nasopharyngeal carcinoma who were treated at Ramathibodi hospital were used in the study. The segmented regions were compared with standard ground truth images from 3 radiologists. In the proposed technique, CT DICOM files are separated into three groups according to their location. This is because common site of tumor is different in each group. Self-organizing maps are generated for each group independently. Because the number of images in group I is small, this thesis focuses only on groups II and III.

In general, DICOM stores CT data in H.U. unit. The range of image intensities may be different because the images may be gained from different sources or acquisitions. Prior to generate SOM network, image in H.U. unit is converted into pixel intensity. The images are then normalized into the similar range.

Proper number of representative image and constant of bound are determined. In the SOM generation, images which their corresponding ratio below 0.5 are excluded. The results showed that 10 representative images and constant of 16 provided highest segmentation performance.

For experiment 2, initial seed is chosen from centroid of each ground truth image. After the segmentation, the segmented region is compared with its corresponding ground truth. Second seed selected from centroid of unsegmented tumor region is then used in the segmentation. The results showed that increasing of seeds provided better segmentation performances. The segmentation results were compared with that of the traditional seeded region growing algorithm. Prior to the comparison, appropriate bound of growing for the traditional approach is determined. The bound of 40 was the best for both groups II and III. The comparison results

showed that the proposed technique was superior to the traditional approach. This is because mode intensity determined from the best matching representative image is used in place of initial seed intensity.

The second part presents the 3D visualization of tumor. Surface rendering and volume rendering are performed. 3D geometry models are developed. They are sliced into 2D images. These models are reconstructed. Their volume is determined by counting the number of voxels and compared with its actual volume. The results showed that volume of the reconstructed models was slightly higher than the actual volume. The last experiment showed the success story of 3D visualization. Tumor model is reconstructed and presented in the skull.

For the future work, the developed software should be tested in the clinical trial for determining the practicability issue. Volume of real tumor should be compared. In addition, satisfaction of radiologists after using the software should be investigated.

REFERENCES

1 Chen J.F. and Lee S.T., “Nasopharyngeal Carcinoma Presenting as an Intracranial Abscess”, Surgical Neurology Vol. 49, Issue 5, pp. 553-557, 2007.

2 WHO, “The Global Burden of Disease : 2004 Update” WHO Library Cataloguing-in-Publication Data. Geneva, Switzerland, 2008.

3 “Anatomy of nasopharynx” http://www.mayoclinicproceedings.com /content/83/4/489/F2.large.jpg.

4 Gillespy T. 3rd, Rowberg AH., “Radiological images on personal computers: introduction and fundamental principles of digital images.”, Digital Imaging, Vol 6, No. 2, pp 81 – 87, 1993.

5 M. J. Duchesne, Francis M., Bernard F. L., and J. Labrie, “A rapid method for converting medical Computed Tomography scanner topogram attenuation scale to Hounsfield Unit scale and to obtain relative density values”, Engineering Geology, Vol. 103, Issues 3-4, pp. 100-105, 2009.

6 D. Reddana, Elliot K. F., “Radiologists’ knowledge and perceptions of the impact of contrast-induced nephropathy and its risk factors when performing computed tomography examinations: A survey of European radiologists” European journal of radiology, Vol. 66, pp. 235-245, 2008.

7 R. C. Gonzalez, R. E. Woods, Steven L. E., “Digital Image Processing Using MATLAB”, Gatesmark Publishing, 2007.

8 C.V. Jiji , P. Neethu, and Subhasis C., “Alias-Free Interpolation”, Lecture Notes in Computer Science, Springer Berlin , Vol. 3954, pp. 255-266, 2006.

9 “CT images in different planes”, http://static.spineuniverse.com/displaygraphic.php /139/dp_planes-BB.gif .

10 Umbaugh S. E., “Computer Vision and Image Processing”, Prentice Hall, NJ, 1998.

11 M. Sezgin and B. Sankur, “Survey over image thresholding techniques and quantitative performance evaluation”, Journal of Electronic Imaging, Vol. 13, No.1, pp. 146–165.

12 N. Otsu, “A threshold selection method from gray-level histograms”, IEEE Transactions on Systems, Man, and Cybernetics, Vol.9, pp. 62–66, 1979

13 P. S. Liao, T.S. Chen, and P. C. Chung , “A Fast Algorithm for Multilevel Thresholding”, Journal of Information Science and Engineering, Vol. 17, No.5, pp. 713–727, 2001.

14 Adams R. and Bischof L., “Seeded Region Growing”, IEEE Transactions on Pattern Analysis and Machine Intelligence, Vol. 16, pp.641-47, 1994.

15 J. Zhou, et al., “MR Tumor Segmentation for Nasopharyngeal Carcinoma Using Knowledge based Fuzzy Clustering”, International Journal of Information Technology, Vol. 8, No. 2, 2002.

16 Huang T.M., Kecman V., and Kopriva I., “Kernel Based Algorithms for Mining Huge Data Sets, Supervised, Semi-supervised, and Unsupervised Learning”, Springer-Verlag, Berlin, Heidelberg, Vol. 260, pp. 96, 2006

17 S. Murugavalli and V. Rajamani, “An Improved Implementation of Brain Tumor Detection Using Segmentation Based on Neuro Fuzzy Technique”, Journal of Computer Science, Vol. 3 No. 11, pp. 841-846, 2007

18 R. B. Dubey et al., “Semi-automatic Segmentation of MRI Brain Tumor”, International Journal on Graphics, Vision and Image Processing, Vol. 9, Issue 4, 2009.

19 W. E. Lorensen and Harvey E. C., “Marching cubes: A high resolution 3D surface construction algorithm” Computer Graphics, Vol. 21, No. 4, pp. 163 – 169. 1987.

20 “Rendering a sphere with Gouraud shading”, http://upload.wikimedia.org/wikipedia/commons/a/af/Gouraud_low_anim.gif

21 J. Kruger and R. Westermann, “Acceleration Techniques for GPU-based Volume Rendering”, Proceedings of the 14th IEEE Visualization, pp. 38, 2003

22 E. Catmull and J. Clark, “Recursively generated B-spline surfaces on arbitrary topological meshes”, Seminal graphics: poineering efforts that shaped the field, Association for Computing Machinery, pp 183 – 188, 1998.

23 K. Matsubara et al., “Contrast resolution in multidetector-row CT with 16 detector rows: phantom study”, Journal of Radiological Physics and Technology, Springer Japan, Vol. 1, No.1, pp. 13-19, 2008

24 Alyassin A.M. et al, "Evaluation of new algorithms for the interactive measurement of surface area and volume", Journal of Medical Physics, Vol. 21, No. 6, 1994.

25 W. J. Schroeder, L. S. Avila, and W. Hoffman, “Visualizing with VTK: A Tutorial”, Kitware Inc., http://noodle.med.yale.edu/seminar/papad/vtk_tutorial.pdf

BIOGRAPHY

NAME	Mr Weerayuth Chanapai
DATE OF BIRTH	10 November 1983
PLACE OF BIRTH	Kamphaengphet, Thailand
INSTITUTIONS ATTENDED	Mahidol University, 2002 - 2006 Bachelor of Science (Physical Therapy) Mahidol University, 2006-2010 Master of Engineering (Biomedical Engineering)
RESEARCH GRANTS	Mahidol University Alumni Association
HOME ADDRESS	219/6 M.5 Nakornchum, Meaung, Kamphaengphet 62000 Tel. 089 – 156 – 0047 E-mail : ramboboy26@hotmail.com
PUBLICATION / PRESENTATION	"การตรวจหาใบหน้าบุคคลด้วยเทคนิค Support Vector Machine" in Proc., CRIT 2007, Nakornpathom, Thailand, 2007. (Best paper award) "SOM Based Adaptive Thresholding Technique for Semi-Automatic NPC Image Segmentation", in Proc., WACBA 2009, Hong Kong, 2009. "ซอฟท์แวร์สำหรับจำแนกเนื้อเยื่อมะเร็งช่องคอหลังโพรงจมูกแบบกึ่งอัตโนมัติจากภาพถ่ายซีที", 2nd price honor from National Engineering 2009

"Adaptive Thresholding based on SOM Technique for Semi-Automatic NPC Image Segmentation" In Proc., ICMLA 2009, USA, Dec. 2009.

"โปรแกรมซอฟท์แวร์สำหรับจำแนกเนื้อเยื่อมะเร็งช่องคอหลังโพรงจมูกจากภาพถ่ายซีทีแบบอัตโนมัติ", หนังสือรับรองการแจ้งข้อมูลลิขสิทธิ์, ทะเบียนข้อมูลเลขที่ ว1. 3232